Please cite this article in press as: Zhu et al., The RALF1–FERONIA Complex Phosphorylates eIF4E1 to Promote Protein Synthesis and Polar Root Hair Growth, Molecular Plant (2019), https://doi.org/10.1016/j.molp.2019.12.014

Molecular Plant
Research Article

CellPress
PARTNER JOURNAL

The RALF1–FERONIA Complex Phosphorylates eIF4E1 to Promote Protein Synthesis and Polar Root Hair Growth

Sirui Zhu[1,7], José Manuel Estévez[2,3,7], Hongdong Liao[1], Yonghua Zhu[1], Tao Yang[4], Chiyu Li[1], Yichuan Wang[5], Lan Li[1], Xuanming Liu[1], Javier Martinez Pacheco[2], Hongwei Guo[5] and Feng Yu[1,6,*]

[1]State Key Laboratory of Chemo/Biosensing and Chemometrics, College of Biology, and Hunan Key Laboratory of Plant Functional Genomics and Developmental Regulation, Hunan University, Changsha 410082, P.R. China

[2]Fundación Instituto Leloir, Buenos Aires C1405BWE, Argentina and IIBBA-CONICET, Buenos Aires C1405BWE, Argentina

[3]Centro de Biotecnología Vegetal, Facultad de Ciencias de la Vida, Universidad Andres Bello, Santiago RM 8370146, Chile

[4]National Engineering Laboratory for Rice and Byproduct Deep Processing, Central South University of Forestry and Technology, Changsha 410004, P.R. China

[5]Institute of Plant and Food Science, Department of Biology, Southern University of Science and Technology, Shenzhen, Guangdong 518055, P.R. China

[6]State Key Laboratory of Hybrid Rice, Hunan Hybrid Rice Research Center, Changsha 410125, P.R. China

[7]These authors contributed equally to this article.

***Correspondence: Feng Yu (feng_yu@hnu.edu.cn)**

https://doi.org/10.1016/j.molp.2019.12.014

ABSTRACT

The molecular links between extracellular signals and the regulation of localized protein synthesis in plant cells are poorly understood. Here, we show that in *Arabidopsis thaliana*, the extracellular peptide RALF1 and its receptor, the FERONIA receptor kinase, promote root hair (RH) tip growth by modulating protein synthesis. We found that RALF1 promotes FERONIA-mediated phosphorylation of eIF4E1, a eukaryotic translation initiation factor that plays a crucial role in the control of mRNA translation rate. Phosphorylated eIF4E1 increases mRNA affinity and modulates mRNA translation and, thus, protein synthesis. The mRNAs targeted by the RALF1–FERONIA–eIF4E1 module include ROP2 and RSL4, which are important regulators of RH cell polarity and growth. RALF1 and FERONIA are expressed in a polar manner in RHs, which facilitate eIF4E1 polar localization and thus may control local *ROP2* translation. Moreover, we demonstrated that high-level accumulation of RSL4 exerts negative-feedback regulation of *RALF1* expression by directly binding the *RALF1* gene promoter, determining the final RH size. Our study reveals that the link between RALF1–FERONIA signaling and protein synthesis constitutes a novel component regulating cell expansion in these polar growing cells.

Key words: eIF4E1, FER, polar cell growth, RALF1, root hairs, RSL4

Zhu S., Estévez J.M., Liao H., Zhu Y., Yang T., Li C., Wang Y., Li L., Liu X., Pacheco J.M., Guo H., and Yu F. (2020). The RALF1–FERONIA Complex Phosphorylates eIF4E1 to Promote Protein Synthesis and Polar Root Hair Growth. Mol. Plant. ■ ■, 1–19.

INTRODUCTION

The identification of the mechanism that determines cell size and shape in response to a change in the environment is a central goal of cell biologists. Changes in cell volume or surface area have profound effects on multiple cellular activities, such as the biosynthetic capacity and nutrient exchange. At the same time, growth is intimately related to shape (Marshall et al., 2012); cells must fit together like puzzle pieces to form tissues and organs, which means that a cell has to fine-tune its size and shape so that it fits into the overall tissue (Marshall et al., 2012).

During growth, the surface of a cell expands through the addition of new material to the membrane or cell wall. Simultaneously, the synthesis of new cytoplasmic content (e.g., proteins) increases the cell's volume (Marshall et al., 2012; Klumpp et al., 2013). Accumulating evidence suggests that protein synthesis occurring in a spatiotemporally controlled fashion could regulate cell size and shape in different

Published by the Molecular Plant Shanghai Editorial Office in association with Cell Press, an imprint of Elsevier Inc., on behalf of CSPB and IPPE, CAS.

Please cite this article in press as: Zhu et al., The RALF1–FERONIA Complex Phosphorylates eIF4E1 to Promote Protein Synthesis and Polar Root Hair Growth, Molecular Plant (2019), https://doi.org/10.1016/j.molp.2019.12.014

organisms (Rodriguez et al., 2008; Marshall et al., 2012; Klumpp et al., 2013; Shigeoka et al., 2016).

Protein synthesis can be divided into three main stages: initiation, elongation, and termination (Sonenberg and Hinnebusch, 2007). The eIF4F complex is a key component involved in translation initiation and determination of the protein synthesis rate. eIF4F consists of eIF4E, which recognizes the mRNA cap, and the scaffolding protein eIF4G, which binds to other factors to recruit the ribosome to the mRNA (Avdulov et al., 2004; Sonenberg and Hinnebusch, 2007). The spatial regulation of translation within the cytoplasm results in the accumulation of newly synthesized proteins in discrete locations in the cell, and this process is critical for polarized cell growth.

Polarized cell growth, a process in which cell length is greatly extended relative to cell width, is crucial to the development and survival of an organism. In animals, plants, and fungi, there are distinct examples of cells that exhibit polarized growth, including neuronal axon, pollen tube, root hair (RH), and fungal hyphae cells (Drubin and Nelson, 1996; Hepler et al., 2001). During the rapid uniaxial extension of cells, rapid protein synthesis and accumulation occurring with spatial precision in the tip growth region are indispensable (Drubin and Nelson, 1996; Rodriguez et al., 2008). In plants, the RHs elongate away from the root surface via growth that is restricted to their tips, known as tip growth (Grierson et al., 2014). RHs undergoing polar growth are believed to play an important role in the absorption of water and nutrients from soil (Datta et al., 2011). Because of their rapid growth and accessibility, RHs are suitable for investigating cell expansion and polarity in relation to protein synthesis. After the specification of hair-producing cells, RH growth can be conceptually separated into two phases: (i) the initiation of RH growth, which leads to the formation of a bulge at a basal position in the cell, and (ii) the slow establishment of tip growth from the bulge, followed by rapid exocytosis of cell-wall and membrane materials localized at the hair tip (Zheng and Yang, 2000; Etienne-Manneville and Hall, 2002; Nibau et al., 2006).

A series of genetic factors have been reported to regulate the differentiation and growth of RHs. *ROOT HAIR DEFECTIVE2* (*RHD2*), an NADPH oxidase that produces reactive oxygen species that induce Ca^{2+} uptake in the tip region of growing RHs (Véry and Davies, 2000; Takeda et al., 2008), and EXPANSIN7 (*EXP7*) have been implicated in RH cell elongation (Cho and Cosgrove, 2002). *KOJAK*, a cellulose synthase-like protein, has been suggested to function in the synthesis of non-cellulosic cell-wall polysaccharides (Favery et al., 2001). *SUPERCENTIPEDE1* (*SCN1*), which encodes a Rho GTPase GDP dissociation inhibitor (RhoGDI), is required for the spatial regulation of growth early in differentiation (Carol et al., 2005), and more importantly, RhoGDI proteins regulate the activity of Rho GTPases in plants (ROPs). ROPs are specifically localized at the future sites of RH initiation, and overexpression of *ROP2* generates additional and misplaced RHs in plants (Molendijk et al., 2001; Jones et al., 2002). At the transcriptional regulatory level, *ROOT HAIR DEFECTIVE6* (*RHD6*) is a basic-helix–loop–helix (bHLH) transcription factor that specifies the position of RH emergence (Menand et al., 2007; Yi et al., 2010), while *LJRHL1-like 3* (*LRL3*) acts downstream of *RHD6*, which positively regulates RH elongation (Karas et al., 2009). *RHD-6-LIKE 4* (*RSL4*) encodes a bHLH transcription factor that regulates hair cell elongation by controlling the expression of hundreds of genes (Yi et al., 2010). More interestingly, the duration of RH growth is determined by the regulation of RSL4 protein synthesis and degradation in RHs and not by its transcriptional level (Datta et al., 2015). In addition to RSL4, the spatially precise *de novo* synthesis of proteins encoded by these RH-related genes (RH genes) must be strictly regulated. However, there is limited evidence explaining how extracellular signals may regulate translation with spatial precision through the protein synthesis machinery in eukaryotic cells.

Plant RAPID ALKALINIZATION FACTORS (RALFs) are secreted peptides that function as extracellular signals and bind to *Catharanthus roseus* RECEPTOR-LIKE KINASE 1-LIKE (*Cr*RLK1L) family members such as FERONIA (FER) (Li et al., 2016; Liao et al., 2017; Franck et al., 2018). RALF1–FER complexes are central regulators of plant cell size and shape that allow plants to respond to environmental changes. Mutations in FER cause a series of defects in growth and polarity of different cell types, such as RH, leaf pavement, and pollen tube cells (Escobar-Restrepo et al., 2007; Li et al., 2016; Liao et al., 2017; Franck et al., 2018). Furthermore, the context-specific roles of RALF1–FER complexes make them excellent models for studying the molecular mechanisms of cell size regulation (Li et al., 2016; Liao et al., 2017; Franck et al., 2018). The RALF peptide, together with components including LORELEI-LIKE GLYCOSYLPHOSPHATIDYLINOSITOL-ANCHORED PROTEIN 1 (Li et al., 2015; Xiao et al., 2019) and EXTRACELLULAR LEUCINE-RICH REPEAT EXTENSINS (Dünser et al., 2019), binds to the FER receptor and further recruits the RPM1-INDUCED PROTEIN KINASE receptor-like kinase (Du et al., 2016), initiating a phosphorylation cascade that promotes *ERBB3–BINDING PROTEIN 1* (*EBP1*) mRNA translation and triggers the nuclear accumulation of EBP1. EBP1 negatively feeds back to FER-mediated RALF1 signaling (Li et al., 2018). Thus, it was suggested that the RALF1–FER complex may regulate protein synthesis and thereby control cell size (Li et al., 2018); however, the underlying mechanisms are unclear.

In this study, we investigated how the RALF1–FER module promotes RH polar growth. We found that FER physically interacts with and phosphorylates eIF4E1, an early translation initiation factor (eIF), at the plasma membrane (PM). The RALF1–FER complex promotes the mRNA translation of RH-specific genes, including *RSL4* and *ROP2*, by facilitating eIF4E1 phosphorylation and its binding with specific mRNAs. These three proteins, RALF1, FER, and eIF4E1, show polar localization in RHs, providing spatial control of localized protein synthesis and determining final RH cell size. Furthermore, we observed that *RALF1* expression is negatively regulated by high levels of RSL4, forming a negative feedback regulatory loop. Our study establishes the molecular links between the RALF1 peptide signal and the regulation of localized protein synthesis in RH cells, suggesting that a precise regulatory mechanism controls cell size and polar growth via transmembrane receptors coupled to extracellular cues such as RALF peptides.

RESULTS

RALF1–FER Promotes the Translation of mRNAs of RH-Specific Genes

To further expand our understanding of how RALF1–FER promotes RH tip growth (Du et al., 2016), we first tested whether

Please cite this article in press as: Zhu et al., The RALF1–FERONIA Complex Phosphorylates eIF4E1 to Promote Protein Synthesis and Polar Root Hair Growth, Molecular Plant (2019), https://doi.org/10.1016/j.molp.2019.12.014

RALF1 could increase FER-mediated RH growth. The treatment of *ralf1-1* mutants (Du et al., 2016) with the exogenous RALF1 peptide at 1 μM rescued the *ralf1-1* RH growth defect, indicating that this treatment mimicked endogenous RALF1 (Supplemental Figure 1A). We then treated wild-type (WT) Col-0 and *fer-4* (*FER* null mutant) (Du et al., 2016) seedling roots with 1 μM RALF1 and found that the treated WT roots exhibited longer RHs than the untreated controls (Figure 1A and 1B), whereas the *fer-4* mutant was insensitive to RALF1 treatment (Supplemental Figure 1A), providing the first indication that RALF1 requires FER to trigger RH growth. Then, we asked whether this specific growth increase requires active protein synthesis. Consistent with previous results (Vijayakumar et al., 2016), treatment with the translation inhibitor cycloheximide (CHX; 8–14 μM) significantly reduced or completely suppressed RH growth (Supplemental Figure 1B). Furthermore, when translation was blocked by treatment with 8 μM CHX, the RHs lost their polarity, resulting in abnormal phenotypes (Figure 1C). CHX treatment in the presence of RALF1 suppressed the RALF1-induced increase in RH growth (Figure 1A and 1B and Supplemental Figure 1C and 1D). We performed CHX treatment for a shorter time twice (4 h/day) within 2 days to block protein synthesis, and we obtained similar results (Supplemental Figure 1E). These data are consistent with the idea that the RALF1–FER pathway requires active protein synthesis to trigger RH growth.

We next measured the abundance of the RALF1–FER pathway-related proteins ROP GTPase (ROP2) (Duan et al., 2010) and EBP1 (Li et al., 2018) with or without RALF1 treatment. RALF1 triggered rapid accumulation of these proteins (Supplemental Figure 1F), even when roots were treated with the transcription inhibitor cordycepin (CRD) (Supplemental Figure 2A–2E). We confirmed the effectiveness of CRD by analyzing the decay rate of the unstable *ARABIDOPSIS ORTHOLOG OF HS1 PRO1-2* (*AtHSPRO2*) mRNA (Gutiérrez et al., 2002) (Supplemental Figure 2A). As expected, CHX blocked RALF1-induced protein accumulation (Supplemental Figures 1F and 2B–2E) and did not alter *ROP2*, *EBP1*, or *AtHSPRO2* mRNA abundance (Supplemental Figure 2A). In addition, RALF1 did not elicit ACTIN protein accumulation (Supplemental Figure 1F). Furthermore, treatment with either low-nutrient-content medium ($^1/_2$-strength Murashige and Skoog) or the PRECURSOR OF PEPTIDE 1 peptide did not induce the accumulation of the ROP2 protein (Supplemental Figure 2F–2I). To rule out the possibility that the upregulation of protein abundance observed in the immunoblot assays resulted from effects on the loading controls (e.g., ACTIN might have different sensitivities to RALF1 in distinct tissues), we compared the expression patterns of *pROP2::ROP2-GFP* in roots that were or were not treated with RALF1 (Supplemental Figure 3A and 3B). RALF1 upregulated ROP2-GFP in both the root epidermis and RH cells (Supplemental Figure 3A and 3B). We therefore speculated that RALF1 modulates protein accumulation in the absence of *de novo* mRNA transcription by influencing mRNA translation.

To further explore the role of the RALF1–FER pathway in *de novo* protein synthesis, we investigated the effect of this pathway on the RSL4 transcription factor. RSL4 protein abundance determines final RH cell size (Datta et al., 2015; Mangano et al., 2017), making RSL4 a prime candidate linking protein synthesis with cell size. However, RALF1 treatment did not upregulate *RSL4* mRNA levels (Figure 1D). We next used the *pRSL4::GFP-RSL4* (GFP-RSL4) transgenic line (Datta et al., 2015) to compare the abundance of RSL4 during RH development with or without RALF1 treatment (Figure 1E and 1F). We detected significantly stronger GFP-RSL4 fluorescence in RH nuclei from cells of different lengths after RALF1 treatment, indicating that RALF1 may promote fast RSL4 protein synthesis (Figure 1E and 1F). To test this possibility, we performed fluorescence recovery after photobleaching (FRAP) experiments (Datta et al., 2015) in which roots were treated with or without RALF1 for 30 min, and the fluorescence recovery of GFP-RSL4 after photobleaching was examined (Figure 1G and 1H). As RALF1 does not affect *RSL4* mRNA, the rate of recovery of GFP-RSL4 fluorescence reflects the *de novo* GFP-RSL4 protein synthesis rate. RALF1 increased the fluorescence recovery rate compared with the control at both the preinitiation and the initiation stages of RH growth. We then performed a nucleus fractionation assay to detect GFP-RSL4 accumulation in the nucleus and the cytoplasm after RALF1 treatment (Figure 1I and 1J). GFP-RSL4 accumulated at similar incremental rates in the nucleus and cytoplasm, again suggesting that RALF1 promotes GFP-RSL4 protein accumulation by regulating overall translation, but not transport from the cytoplasm to the nucleus. These data suggest that RALF1–FER modulates the translation of RSL4 and other RH-related proteins to regulate RH growth and shape.

We then tested whether FER is required for the RALF1-mediated modulation of mRNA translation. Polysome profiling analysis for assessing the effect of RALF1 on the translation of RH genes with specific roles in the initiation and elongation phases of RH growth (Datta et al., 2015; Vijayakumar et al., 2016; Mangano et al., 2017) showed that RALF1 promotes the translation of several RH-related genes (i.e., *ROP2/6*, *RSL4*, *EXP7*, *RHD6*, *SCN1*, and *KOJAK*), but not others (i.e., *GUANINE NUCLEOTIDE EXCHANGE FACTORS* [*GEF1/10*], *RHD2*, and *LRL3*) in the WT (Figure 2A and 2B). The lack of *FER* in *fer-4* plants caused the appearance of an extra 60S peak between the 40S and the 80S peaks in polysome profiling assays and a decrease in the intensity of polysomal fractions (Figure 2A and 2B), indicating that shows ribosome synthesis is greatly altered in *fer-4*. Moreover, the RALF1-mediated activation of the translation of some RH-related mRNAs was blocked in *fer-4* (Figure 2A and 2B).

FER Interacts with and Phosphorylates eIF4E1

Previous yeast two-hybrid (Y2H) and immunoprecipitation–mass spectrometry (IP–MS) screens (Mao et al., 2015; Chen et al., 2016; Du et al., 2016) showed that FER interacts with multiple components of the cell translational machinery, including eIFs, translation elongation factors, and small and large ribosomal subunit proteins (Supplemental Figure 4A). Y2H and pull-down assays confirmed that most of the eIFs (e.g., eIF3G, eIF4Es) interact with FER (Supplemental Figure 4B and 4C). We cloned four eIF4E gene family members (Patrick and Browning, 2012) (i.e., *eIF4E1*, *eIF(iso)4E*, *eIF4E1b*, and *eIF4E1c*) into an activation domain (AD) vector and the FER cytosolic domain (FER–CD) into a binding domain (BD) vector and tested their interaction (Figure 3A and Supplemental Figure 4B). Y2H assays showed that all four eIF4Es interact with FER–CD in yeast

Please cite this article in press as: Zhu et al., The RALF1–FERONIA Complex Phosphorylates eIF4E1 to Promote Protein Synthesis and Polar Root Hair Growth, Molecular Plant (2019), https://doi.org/10.1016/j.molp.2019.12.014

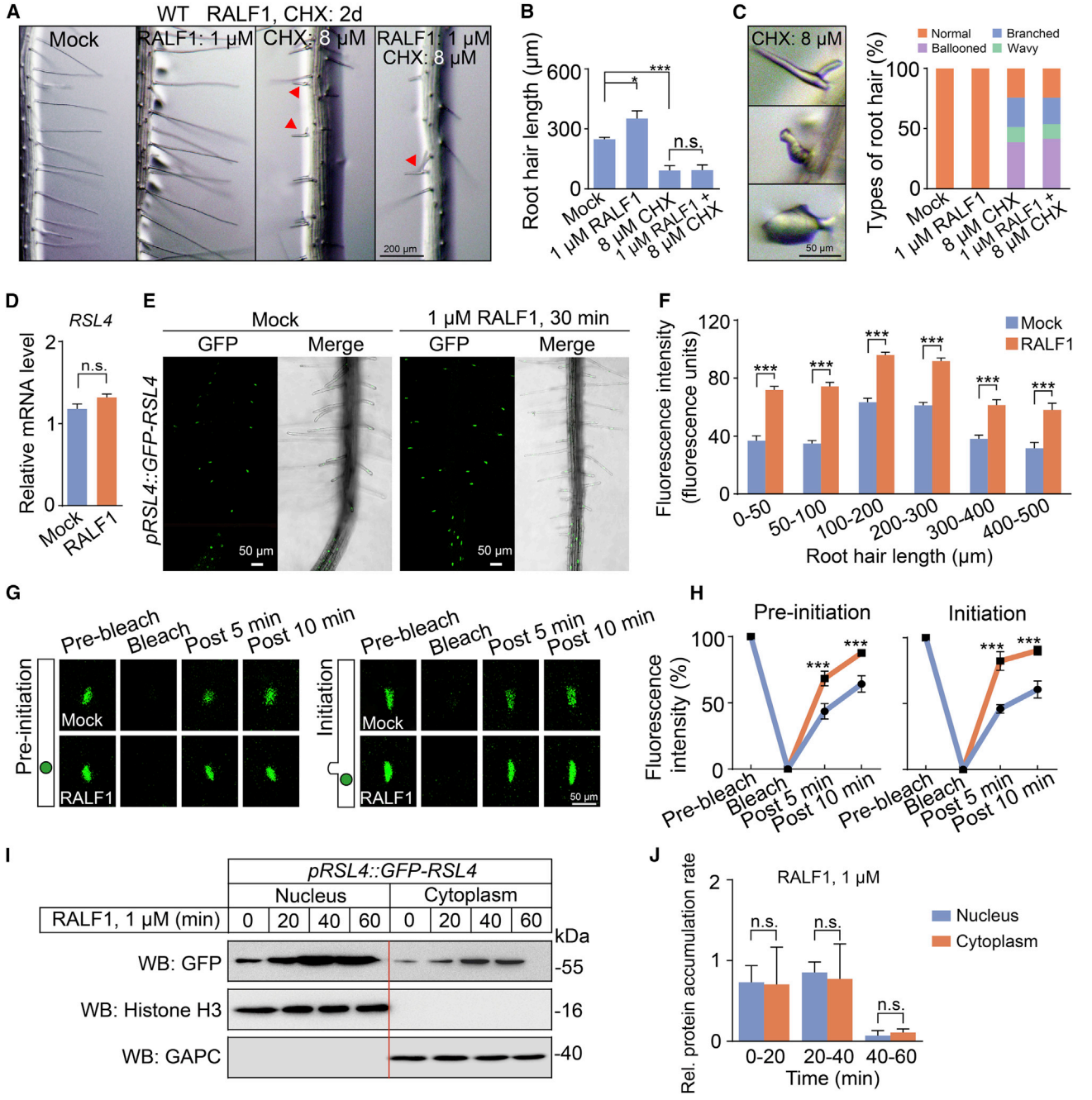

Figure 1. RALF1–FER Modulates the Translation of RSL4.

(A) Representative images of RHs. Red arrows indicate branched RHs.

(B) Average lengths of RHs from **(A)** (160 RHs from eight roots).

(C) Abnormal morphologies and percentage of RH cells with each type of shape in CHX-treated roots (100 RHs from 10 roots per genotype).

(D) RT-qPCR analysis of *RSL4* with or without RALF1 (1 μM, 30 min) treatment.

(E) Fluorescence of GFP-RSL4 with or without RALF1.

(F) Quantification of the fluorescence intensity of RHs of different lengths in **(E)**; 50 RH cells from five growing roots were observed.

(G) FRAP assay of GFP-RSL4 at the preinitiation and initiation stages. The models on the left correspond to RH cells in the two growth stages; the green ellipse indicates the RSL4 protein.

(H) Statistical analysis of fluorescence recovery in **(G)**; 20 RH cells from four growing roots were observed.

(I and J) RALF1-induced RSL4 protein accumulation in the nuclear and cytoplasmic fractions. The relative levels of RSL4 protein accumulation in the nucleus and cytoplasm were analyzed using ImageJ.

At least three biological replicates of **(A)**–**(J)** were performed with similar results. Data are shown as the mean ± SD; $^{*}p < 0.05$, $^{***}p < 0.001$, n.s., non-significant by one-way ANOVA.

Please cite this article in press as: Zhu et al., The RALF1–FERONIA Complex Phosphorylates eIF4E1 to Promote Protein Synthesis and Polar Root Hair Growth, Molecular Plant (2019), https://doi.org/10.1016/j.molp.2019.12.014

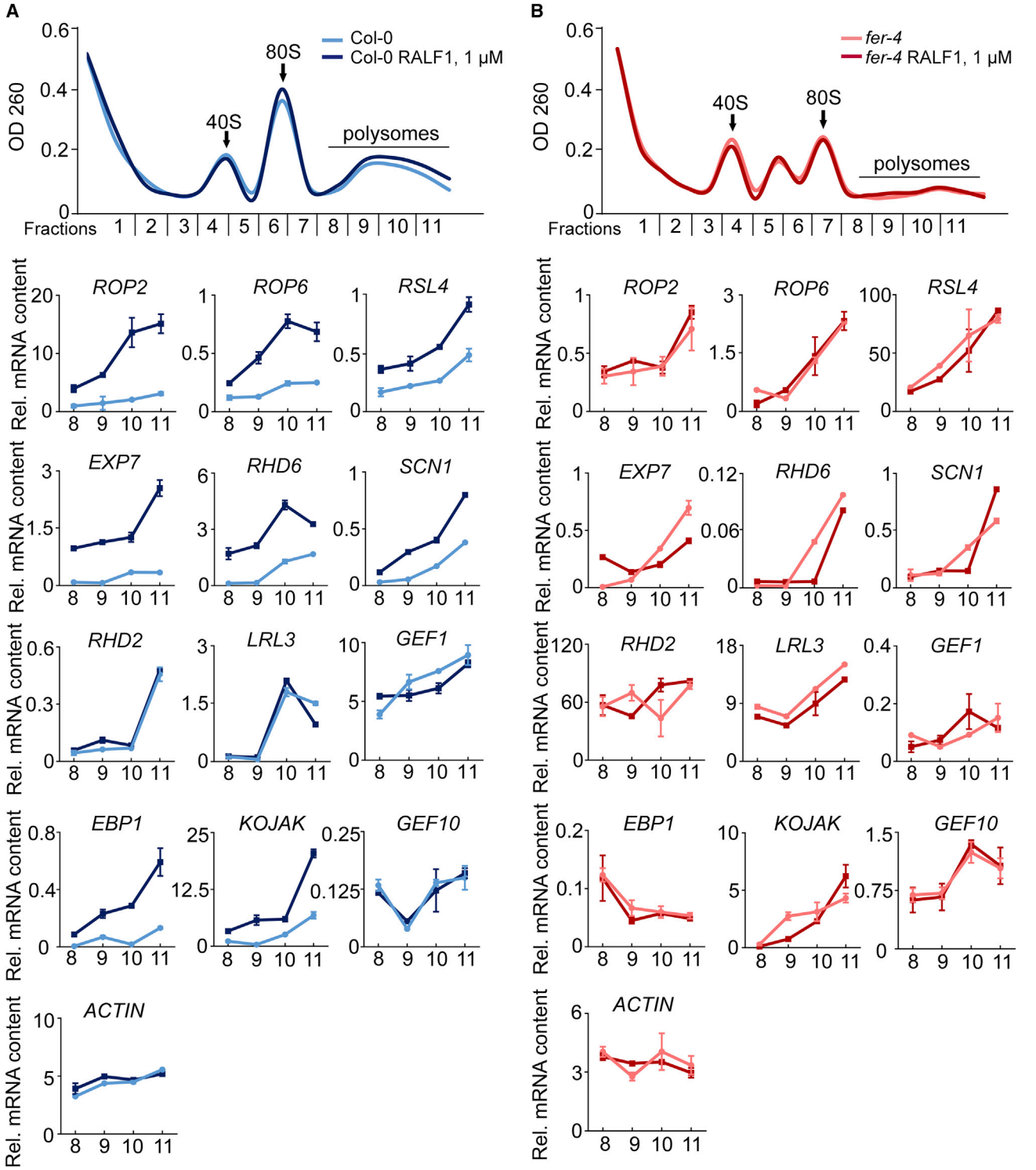

Figure 2. RALF1 Affects the Translation of RH Tip Growth-Related Gene Transcripts.

(A and B) Top: ribosome profiles. Fractions (8–11) containing mRNAs associated with polysomes are indicated with a black line. Bottom: RT-qPCR results for polysome-associated mRNAs. At least three biological replicates of **(A)–(B)** were performed with similar results.

(Figure 3A and Supplemental Figure 4B). We then confirmed the interaction of GST-eIF4E1, GST-eIF(iso)4E, and GST-eIF3G with His-FER-CD using glutathione S-transferase (GST) pull-down assays (Figure 3B and Supplemental Figure 4C). Therefore, we focused on examining FER–eIF4E1 interactions using *in vivo* assays. Bimolecular fluorescence complementation (BiFC) and co-immunoprecipitation (coIP) assays were first used to confirm the expression of the selected proteins and showed that eIF4E1 interacts with FER in the *Arabidopsis thaliana* PM (Figure 3C, Supplemental Figure 4D and 4E). In addition,

Please cite this article in press as: Zhu et al., The RALF1–FERONIA Complex Phosphorylates eIF4E1 to Promote Protein Synthesis and Polar Root Hair Growth, Molecular Plant (2019), https://doi.org/10.1016/j.molp.2019.12.014

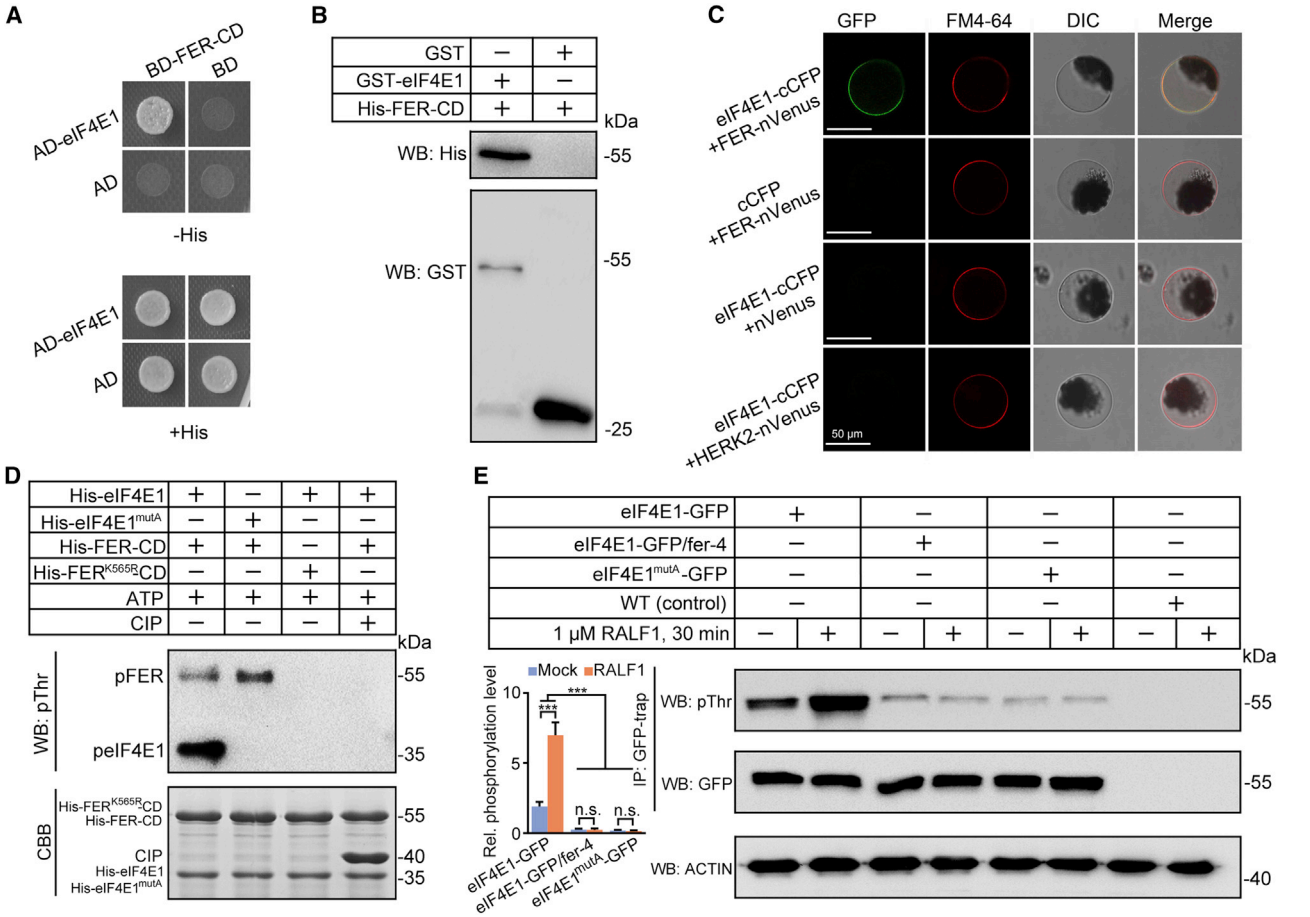

Figure 3. FER Interacts with and Phosphorylates eIF4E1.

(A) Y2H assays showing the eIF4E1–FER interaction. Synthetic dropout medium (–His) containing 20 mM 3-amino-1,2,4-triazole was used to test the interaction.

(B) GST pull-down assay showing that eIF4E1 interacts with FER.

(C) eIF4E1 interacts with FER in protoplasts in a BiFC assay. Red, FM4-64 membrane dye.

(D) His-FER–CD, but not its kinase-dead form (His-FER^{K565R}–CD), phosphorylates His-eIF4E1 *in vitro*, as detected using a phosphorylated threonine antibody (pThr).

(E) *In vivo* phosphorylation assay. The pThr antibody signal indicates the phosphorylation status of eIF4E1 before and after RALF1 (1 μM, 30 min) treatment. The relative phosphorylation level was analyzed using ImageJ.

At least four biological replicates were performed for each assay, with similar results. Data are presented as the mean ± SD; ***$p < 0.001$, n.s., non-significant by one-way ANOVA.

eIF4E1 interacts with only a few *Cr*RLK1L gene family members, surprisingly not including ERULUS, an RH-specific receptor-like kinase (Supplemental Figure 4F). Collectively, these results indicate that FER physically interacts with several eIFs, including eIF4E1.

To test whether FER phosphorylates eIF4E1, we used the purified FER cytosolic domain (His-FER–CD), kinase-dead FER–CD (His-FER^{K565R}–CD) (Du et al., 2016; Li et al., 2018), and His-eIF4E1 in an *in vitro* phosphorylation assay. His-FER–CD, but not His-FER^{K565R}–CD, phosphorylated His-eIF4E1 (Figure 3D). We identified the phosphorylation sites of eIF4E1 regulated by FER using our previously developed abscisic acid (ABA)-induced co-expression system (Li et al., 2018), in which PYL1, ABI1, FER–CD, and eIF4E1 (PYL1/ABI1/FER–CD/eIF4E1) were co-expressed in an *Escherichia coli* strain. ABI1 inhibits FER activity to thwart FER phosphorylation of its substrate. When ABA was added to the culture medium, the PYL1–ABA complex interacted with and inhibited ABI1 activity, thus releasing the active FER–CD kinase (Li et al., 2018). Electrospray ionization–MS analysis indicated that after ABA induction, FER phosphorylates eIF4E1 at Ser^{65}, Thr^{67}, Tyr^{118}, Thr^{140}, and Thr^{188} (Supplemental Figure 5A–5D). A mutant in which all five sites were mutated to Ala (eIF4E1^{mutA}) was not phosphorylatable by FER (Figure 3D), confirming that all five phosphorylation sites are relevant *in vitro*. In addition, after the generation of the *eIF4E1-GFP*, *eIF4E1^{mutA}-GFP*, and *eIF4E-GFP/fer-4* transgenic lines in the WT background, we determined that RALF1 promoted the FER-mediated phosphorylation of eIF4E1 in *eIF4E1-GFP* plants, whereas *eIF4E-GFP/fer-4* and *eIF4E1^{mutA}-GFP* plants presented much weaker phosphorylation signals with or without RALF1 treatment (Figure 3E). Furthermore, endogenous eIF4E1 phosphorylation levels were much lower in the *fer-4* mutant than in the WT. *fer-4/gFER-FER^{K565R}* (Haruta

Please cite this article in press as: Zhu et al., The RALF1–FERONIA Complex Phosphorylates eIF4E1 to Promote Protein Synthesis and Polar Root Hair Growth, Molecular Plant (2019), https://doi.org/10.1016/j.molp.2019.12.014

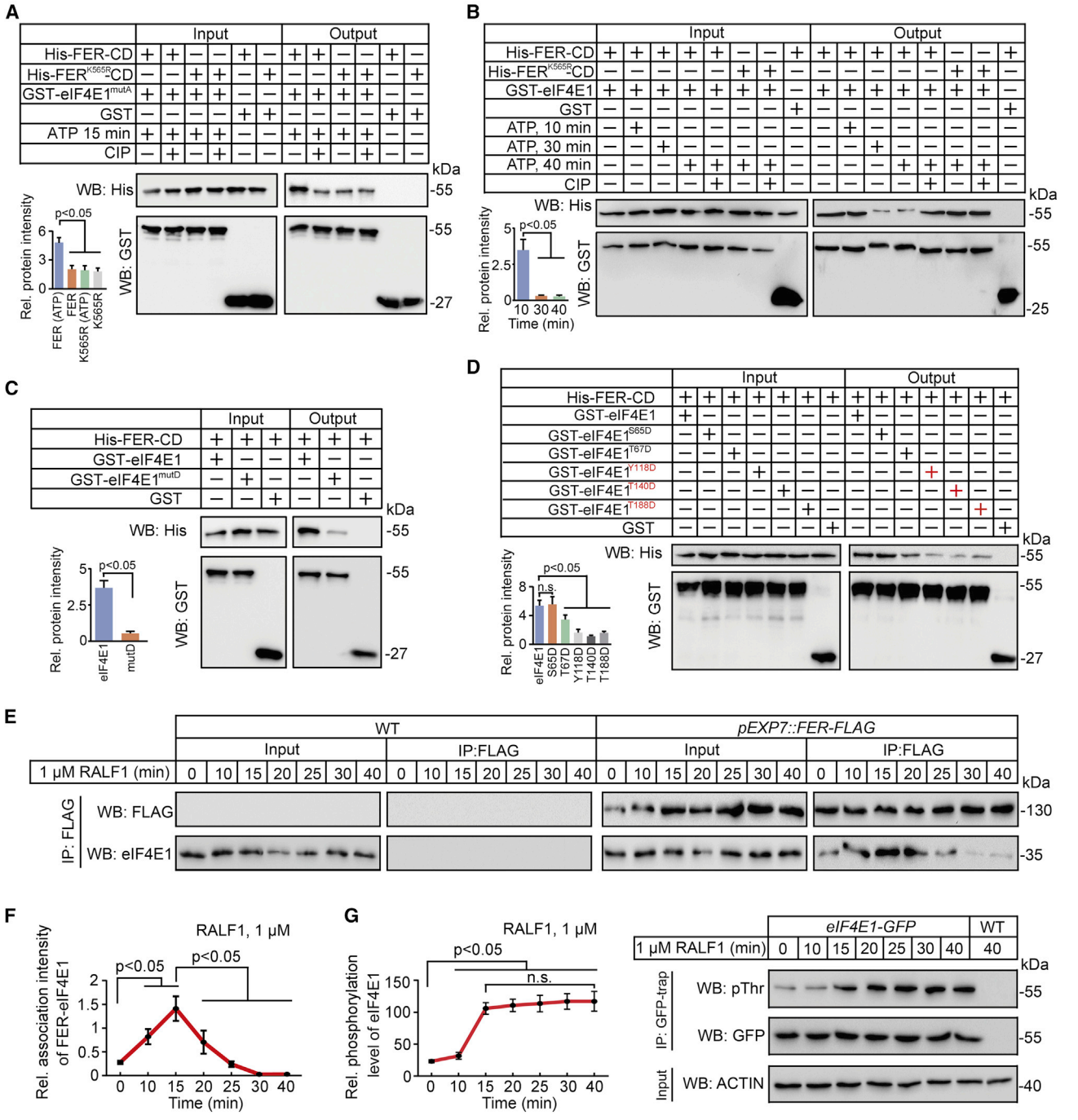

Figure 4. The FER–eIF4E1 Interaction Is Regulated by the Phosphorylation of FER and eIF4E1.

(A) Phosphorylated FER (ATP 15 min) exhibits a higher affinity toward eIF4E1^{mutA}. The relative protein intensity of His-FER–CD in the output was analyzed using ImageJ.

(B) GST pull-down assay. Phosphorylated eIF4E1 (ATP 30 min, ATP 40 min) shows a weaker interaction with His-FER–CD. The relative protein intensity of His-FER–CD in the output was analyzed using ImageJ.

(C) GST pull-down assay. The eIF4E1^{mutD} form shows weaker interaction with His-FER–CD than does eIF4E1. The relative protein intensity of His-FER–CD in the output was analyzed using ImageJ.

(D) Phosphorylation site single-point mutations partially impair the FER-eIF4E1 interaction. The relative protein intensity of His-FER–CD in the output was analyzed using ImageJ.

(E and F) RALF1 (1 μM) affects the FER–eIF4E1 association in RHs. Short-term RALF1 treatment increases the FER–eIF4E1 interaction and upregulates eIF4E1 phosphorylation. Phosphorylated eIF4E1 is then released from FER (at the PM) after 15 min, reducing the FER–eIF4E1 interaction. The relative

(legend continued on next page)

Please cite this article in press as: Zhu et al., The RALF1–FERONIA Complex Phosphorylates eIF4E1 to Promote Protein Synthesis and Polar Root Hair Growth, Molecular Plant (2019), https://doi.org/10.1016/j.molp.2019.12.014

et al., 2018) exhibited low levels of eIF4E1 phosphorylation (Supplemental Figure 5E), which is consistent with the observation that FER^{K565R} still functions to some extent in plants in other biological contexts (Haruta et al., 2018). These results indicate that RALF1 stimulation increased the FER-mediated phosphorylation of eIF4E1 at multiple sites.

Interaction between FER and eIF4E1 Is Regulated by Reciprocal Phosphorylation

To determine the effect of eIF4E1 phosphorylation on the FER–eIF4E1 association, we first tested whether the FER–eIF4E1 association is regulated by FER phosphorylation. To rule out disturbances caused by eIF4E1 phosphorylation, we used $eIF4E1^{mutA}$ as the substrate to compare the affinity of FER (ATP) (which activates FER self-phosphorylation) and FER^{K565R} (ATP) for the substrate (Figure 4A). We found that FER (ATP) showed a higher affinity toward $eIF4E1^{mutA}$ than the kinase-dead form FER^{K565R} (ATP). In addition, calf intestinal alkaline phosphatase reduced the interaction of FER (ATP) with $eIF4E1^{mutA}$ but resulted in no alteration of the interaction of FER^{K565R} (ATP) with $eIF4E1^{mutA}$ (Figure 4A). These data indicate that the upregulation of FER phosphorylation increases the FER–eIF4E1 association (Figure 4A). Then, we tested the effect of eIF4E1 phosphorylation on this interaction. FER kinase domain gel-shift assays showed that ATP significantly upregulated both FER and eIF4E1 phosphorylation levels (Figure 4B) after 30-min and 40-min treatments. When FER and eIF4E1 phosphorylation levels were upregulated, the FER-eIF4E1 association was reduced (Figure 4B). Comparison of the interaction between FER and two forms of eIF4E1, WT eIF4E1 and $eIF4E1^{mutD}$ (a phospho-mimetic version of eIF4E1 in which the five phosphorylation sites are mutated to Asp) revealed that $eIF4E1^{mutD}$ exhibited a lower association with FER than WT eIF4E1 (Figure 4C). Next, we mutated each of the five eIF4E1 phosphorylation sites to Asp (D) to compare how they affected the FER–eIF4E1 association. Mutants with phosphorylation-site mutations at Tyr^{118} and Thr^{140} and, to a lower extent, Thr^{188} showed a much weaker interaction with FER than did WT eIF4E1 (Figure 4D). Taken together, the results indicate that the phosphorylation of FER upregulates the FER–eIF4E1 association, and the complete phosphorylation of eIF4E1 then reduces its affinity toward FER.

To confirm this possibility, we expressed *FER* under the control of the RH-specific *EXPANSIN7* promoter (Mangano et al., 2017) (*EXP7*; *pEXP7::FER-FLAG*). CoIP assays showed that RALF1 administration promoted the recruitment of eIF4E1 to FER within 15 min, but the interaction between FER and eIF4E1 became weak from 20 to 40 min (Figure 4E and 4F). In addition, we monitored *in vivo* eIF4E1–GFP phosphorylation over time after RALF1 treatment and showed that eIF4E1 phosphorylation peaked at 15 min (Figure 4G), consistent with the RALF1 treatment affecting the FER–eIF4E1 association within 15 min (Figure 4E and 4F). These results suggest that short-term (15 min) RALF1 treatment increases the FER–eIF4E1 interaction by quickly upregulating FER phosphorylation and that long-term treatment (>15 min) upregulates the phosphorylation of eIF4E1, thereby reducing its interaction with FER; thus, phosphorylated eIF4E1 may be released from FER (at the PM).

FER-Mediated Phosphorylation of eIF4E1 Increases Its mRNA-Binding Ability

In mammals, the phosphorylation of eIF4B at Ser^{422} results in more efficient recruitment of the eIF3 complex, and the eIF3 pre-initiation complex acts as a scaffold to promote efficient protein synthesis (Shahbazian et al., 2016). From the eIF4E1-7-methyl-GDP co-crystal structure homology model (Delano Scientific; Roy et al., 2010), we found that Thr^{140} is located close to the putative position of the mRNA ligand and that Tyr^{118} can directly interact with the mRNA cap (Figure 5A–5C). These observations strongly support our finding that eIF4E1 mutants with phosphorylation-site mutations at Tyr^{118} and Thr^{140} have much weaker interactions with FER than WT eIF4E1 (Figure 4D). To test the possibility that the phosphorylation of eIF4E1 regulates its mRNA-binding ability, we first compared the cap-binding ability of phosphorylated eIF4E1 (GST-peIF4E1) and non-phosphorylated eIF4E1 (GST-eIF4E1) using 7-methyl-GTP (m^7GTP) pull-down assays (Figure 5D). γ-aminophenyl-m^7GTP is an analog of the mRNA cap structure that can bind and be used to further purify the eIF4E1 protein (Tomoo et al., 2002). As expected, peIF4E1 bound to m^7GTP Sepharose resin more quickly and displayed a stronger affinity toward m^7GTP than the non-phosphorylated form of eIF4E1 (Figure 5D). Fluorescence titration experiments were performed for further comparison of the cap-binding affinity of peIF4E1 and $eIF4E1^{mutD}$ with eIF4E1. These experiments showed that peIF4E1 and $eIF4E1^{mutD}$ exhibited a higher binding affinity for the cap analogs compared with eIF4E1 (Figure 5E). In agreement with this, the phosphorylated residues are adjacent to Trp residues that are essential for mRNA cap-binding activity (Supplemental Figure 6) (Sonenberg and Hinnebusch, 2007).

Because the scaffolding protein eIF4G binds to eIF4E and increases eIF4E binding to the mRNA cap *in vitro* (Haghighat and Sonenberg, 1997), we tested whether the FER-mediated phosphorylation of eIF4E1 regulates the eIF4E1–eIF4G interaction. Based on the solved canonical and non-canonical eIF4E-binding motif of *Cucumis melo* eIF4G (*Cm*eIF4G) (Miras et al., 2017), we cloned the motif (865–954 aa) from *A. thaliana* eIF4G (*At*eIF4G). We then analyzed the ability of $GST\text{-}eIF4G^{(865\text{-}954)}$ to interact with phosphorylated eIF4E1 (His-peIF4E1), $eIF4E1^{mutD}$, and non-phosphorylated eIF4E1 (His-eIF4E1) using GST pull-down assays (Figure 5F and 5G). We observed that His-peIF4E1 and $His\text{-}eIF4E1^{mutD}$ exhibited a higher affinity for $eIF4G^{(865\text{-}954)}$ than did His-eIF4E (Figure 5F and 5G). These findings highlight the impact of the eIF4E1 phosphorylation status on the interaction with eIF4G and its impact on mRNA cap binding.

association intensity analyzed with ImageJ. To analyze the total FER content (including phosphorylated and dephosphorylated forms) in a single band, we modified the running conditions (see Methods).

(G) *In vivo* phosphorylation assay. The pThr antibody signal indicates the phosphorylation status of eIF4E1 at 40 min after RALF1 (1 μM) treatment. The relative phosphorylation intensity was analyzed with ImageJ.

At least three biological replicates of **(A)–(G)** were performed, with similar results. Data are presented as the mean ± SD; n.s., non-significant by one-way ANOVA.

Please cite this article in press as: Zhu et al., The RALF1–FERONIA Complex Phosphorylates eIF4E1 to Promote Protein Synthesis and Polar Root Hair Growth, Molecular Plant (2019), https://doi.org/10.1016/j.molp.2019.12.014

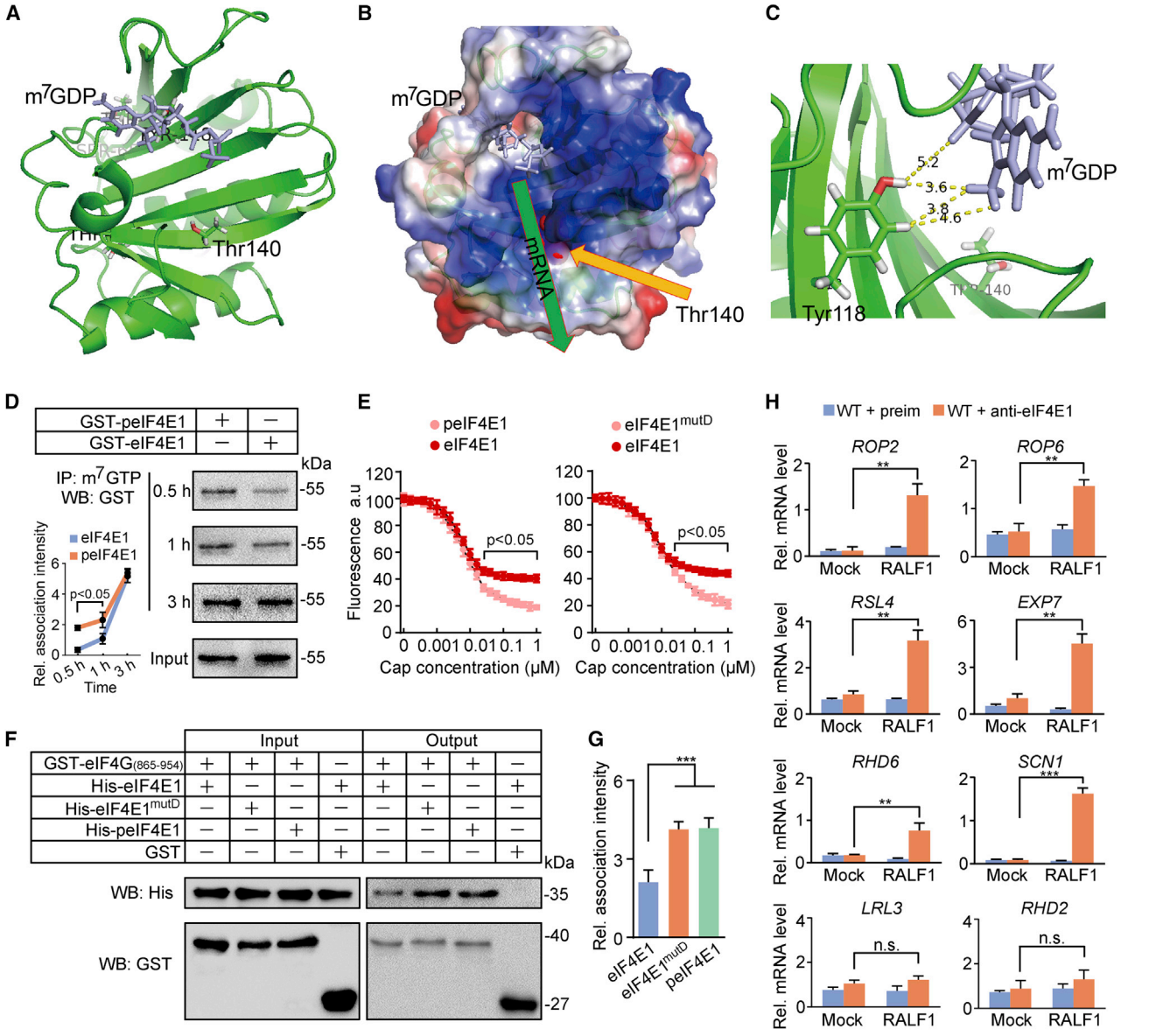

Figure 5. RALF1–FER-Mediated Phosphorylation of eIF4E1 Affects Its Ability to Bind eIF4G and Specific RH mRNAs.

(A) Ribbon diagram of AteIF4E1 in complex with the m^{7}GDP analog (modeled in PyMOL). m^{7}GDP is located in the cap-binding pocket. The Thr^{140} residue is labeled.

(B) The structure of AteIF4E1 is colored according to the electrostatic potential, with the location of Thr^{140} being highlighted. The putative pathway of mRNA extension past Thr^{140} is indicated with a green arrow.

(C) Residue Tyr^{118}, whose phosphorylated form may influence cap binding, is shown in the stick representation.

(D) m^{7}GTP pull-down assay. The m^{7}GTP cap analog was incubated with eIF4E1 or peIF4E1, and the cap-binding ability was assessed at 0.5, 1, and 3 h. The relative association intensity was analyzed using ImageJ.

(E) Fluorescence intensity data for the cap-eIF4E1 titration experiment. Both forms of eIF4E1 (0.1 μM) were titrated with m^{7}GTP, and fluorescence was monitored at 337 nm.

(F and G) GST pull-down assay. The relative association intensity was analyzed using ImageJ.

(H) RIP followed by RT-qPCR indicated that RALF1 (1 μM, 30 min) affects the mRNA-binding ability of eIF4E1.

At least four biological replicates were performed for each assay, with similar results. Data are presented as the mean ± SD; $^{**}p < 0.01$, $^{***}p < 0.001$, n.s., non-significant by one-way ANOVA.

We further tested whether RALF1 affects the *in vivo* mRNA-binding ability of eIF4E1 using an RNA IP (RIP) assay. After RALF1 treatment, high levels of eIF4E1 bound to specific mRNAs of RH genes (i.e., *ROP2/6*, *RSL4*, *EXP7*, *RHD6*, *SCN1*, *KOJAK*, and *EBP1*), but not to other mRNAs (i.e., *LRL3*, *RHD2*, *GEF1/10/14*, and *ACTIN*) (Figure 5H and Supplemental Figure 7A). We next examined the polyribosome profiles of transfer DNA insertion mutants of two *eIF4E* genes, *eif4e1* (At4g18040) and *eif(iso)4e* (At5g35620) (Patrick and Browning, 2012), and the double mutant *eif4e1 eif(iso)4e* (*4e/iso*) (Supplemental Figure 8A–8C), notely, different

Please cite this article in press as: Zhu et al., The RALF1–FERONIA Complex Phosphorylates eIF4E1 to Promote Protein Synthesis and Polar Root Hair Growth, Molecular Plant (2019), https://doi.org/10.1016/j.molp.2019.12.014

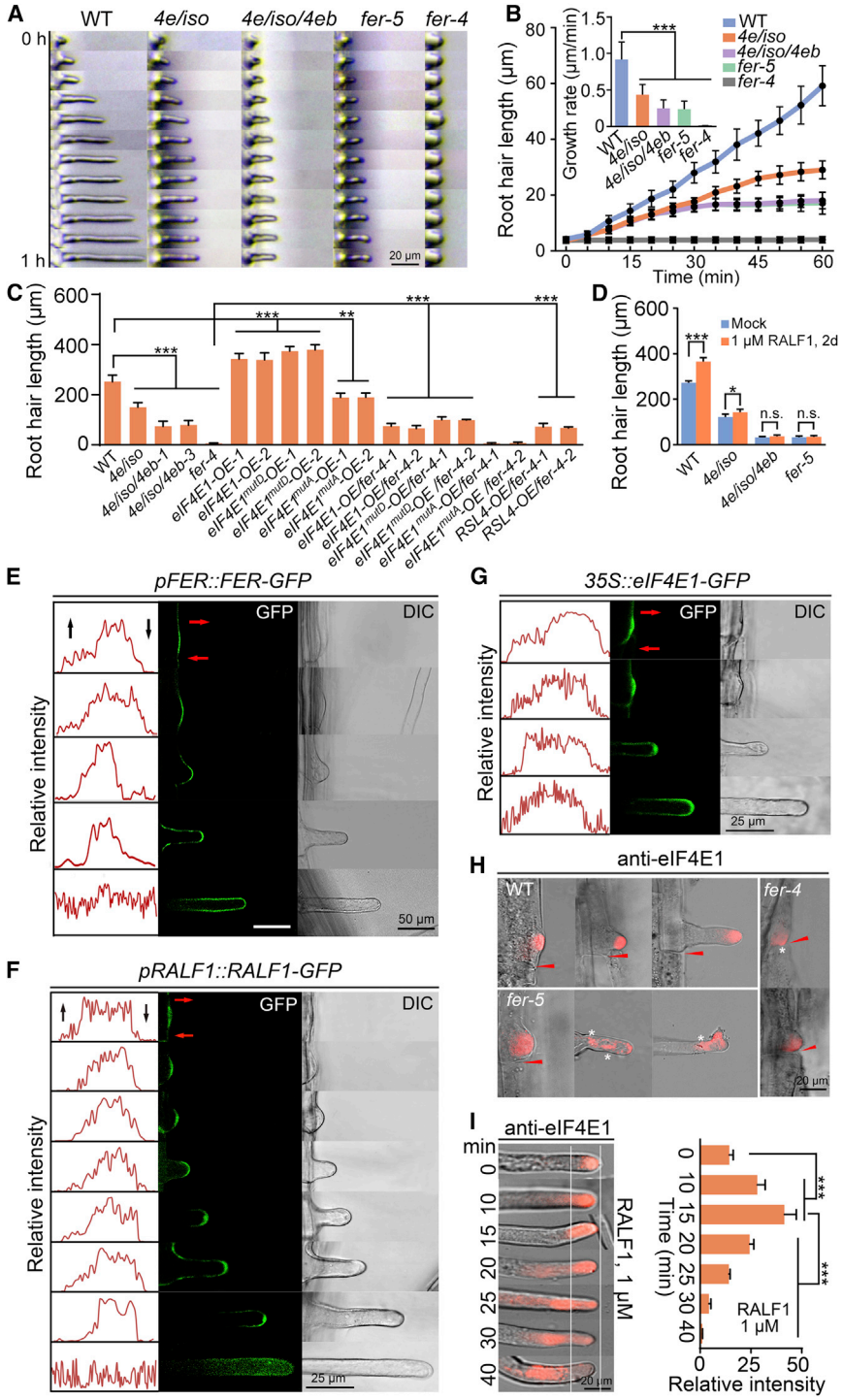

Figure 6. eIF4E1 Functions Downstream of RALF1–FER to Regulate Cell Size.

(A) Growth dynamics of individual RHs; consecutive frames followed for 1 h for one representative RH of each line are shown.

(B) Average growth curve and growth rate (inset) of RHs in **(A)**; 36 RHs from nine growing roots of each line were observed.

(C) Statistical analysis of average RH lengths measured from 80–160 RHs (n = 8 roots per genotype).

(D) Statistical analysis of RALF1-induced RH growth. The lengths of 50 RHs (n = 5 roots per genotype) were measured.

(E–G) Right: representative images of different growth stages of RHs expressing *pFER::FER-GFP*, *pRALF1::RALF1-GFP*, and *35S::eIF4E1-GFP* in the WT background. Left: intensity plots along the PM. Red and black arrows indicate the initial and terminal points of signal accumulation at the PM.

(H) Immunofluorescence assays of eIF4E1. Red triangles, basal ends of trichoblasts; white asterisks, abnormal protein localization.

(I) Left: time-series immunofluorescence assays of eIF4E1 with or without RALF1 treatment. Right: statistical analysis of the fluorescence intensity in the tip area; 30 RHs from 10 growing roots were observed, and the two white lines indicate the signal accumulation area.

At least three biological replicates of **(A)**–**(I)** were performed, with similar results. Data are presented as the mean ± SD; $^{*}p < 0.05$, $^{**}p < 0.01$, $^{***}p < 0.001$ by one-way ANOVA.

from previous work (Bastet et al., 2019), the reason we can get *4e/iso* double mutant is that our mutant is knock-down mutant. The *4e/iso* mutations blocked the RALF1-mediated activation of the same specific mRNAs of RH genes tested previously (Supplemental Figure 7B), suggesting that RALF1 increases the ribosome occupancy of its target mRNAs through the FER–eIF4E1 pathway. We next determined the protein synthesis rates of ROP2 (Abiocode, Q38919; Xu et al., 2014) and EBP1 (Li et al., 2018) and found that their protein levels were lower in the *4e/iso* line and higher in the *eIF4E1-OE* line than in the WT (Supplemental Figure 7C and 7D). These results indicate that RALF1-mediated regulation of the mRNA-binding ability of eIF4E1 regulates the translation rates of several RH-related mRNAs.

eIF4E1 Is Required for RALF1–FER Pathway-Mediated Regulation of RH Size and Polarity

We then analyzed the expression levels of *eIF4Es*, *eIF4G*, and *FER* during several stages of RH development using bioinformatics resources (http://bar.utoronto.ca/eplant/, Waese et al., 2017 and https://software.broadinstitute.org/morpheus/), and we found that *eIF4E1*, *eIF(iso)4E*, *eIF4G*, and *FER* exhibited the highest expression in the RH epidermis differentiation zone (Supplemental Figure 8D). To address whether eIF4Es are required for the RALF1–FER pathway regulation of RH cell size, we investigated the RH phenotypes of *eif4e1*, *eif(iso)4e*, and *4e/iso* and found that only the double *4e/iso* mutant presented shorter RHs than the WT (Figure 6A–6C and Supplemental Figure 9C) ($80 < n < 160$, $p < 0.01$). We then created a triple mutant, *eif4e1 eif(iso)4e eif4e1b* (*4e/iso/4eb*), via CRISPR-Cas9 knockout of the *eIF4e1b* (At1g29550) gene in the *4e/iso* background (Supplemental

Please cite this article in press as: Zhu et al., The RALF1–FERONIA Complex Phosphorylates eIF4E1 to Promote Protein Synthesis and Polar Root Hair Growth, Molecular Plant (2019), https://doi.org/10.1016/j.molp.2019.12.014

Figure 9A and 9B). The *4e/iso/4eb* triple mutation profoundly affected RH growth, yielding a phenotype comparable to that of *fer-5* (*FER* knockdown mutant) (Duan et al., 2010) (Figure 6A–6C and Supplemental Figure 9C). After bulge formation, WT RHs switched to tip growth, showing a constant growth rate of 0.92 ± 0.29 μm/min, whereas *4e/iso* RHs grew at 0.43 ± 0.14 μm/min and *4e/iso/4eb* at 0.24 ± 0.11 μm/min, which was a similar growth rate compared with that observed in *fer-5* (Duan et al., 2010) (0.23 ± 0.13 μm/min), whereas *fer-4* (0.002 ± 0.0004 μm/min) RHs did not grow at all (Figure 6A and 6B). In contrast to the WT, the *4e/iso/4eb* mutants were insensitive to RALF1 in the RH growth assays, whereas *4e/iso* still exhibited some remaining activity (Figure 6D and Supplemental Figure 9G). Furthermore, the *4e/iso* and *4e/iso/4eb* mutants frequently lost normal RH morphology (Supplemental Figure 9H). In contrast, plants from the *eIF4E1*-overexpressing lines *eIF4E1-OE* and *eIF4E1^{mutD}-OE* presented longer RHs than the WT (Figure 6C and Supplemental Figure 9C and 9D). We measured the growth rate of *eIF4E1-OE* plants (1.25 ± 0.4 μm/min) and found that it was faster than that of WT (0.93 ± 0.3 μm/min) (Supplemental Figure 9E and 9F). In contrast, *eIF4E1^{mutA}-OE*, in which eIF4E1 is not phosphorylatable by FER, exhibited shorter RHs than the WT (Figure 6C and Supplemental Figure 9C). Thus, the FER-mediated phosphorylation of eIF4E1 is important for eIF4E1-regulated RH growth. When expressed in the *fer-4* background, *eIF4E1^{mutD}-OE*, *eIF4E1-OE*, and *RSL4-OE* partially rescued the RH length defects of the *fer-4* mutant (Figure 6C and Supplemental Figure 9C). However, *eIF4E1^{mutA}-OE* did not rescue the RH defects of *fer-4* (Figure 6C and Supplemental Figure 9C; $p > 0.05$). The hypothesis that eIF4E1 is a target and effector of FER has been further supported by assays quantifying rosette size (Duan et al., 2010; Du et al., 2016) and pavement cell shape (Du et al., 2016) (Supplemental Figure 10) and RALF1-regulated primary root growth assays (Du et al., 2016; Li et al., 2018) (Supplemental Figure 11), which have indicated that FER is a global regulator of cell size and shape (Liao et al., 2017; Franck et al., 2018; Li et al., 2018). These results indicate that eIF4E1 abundance and phosphorylation status control cell size and shape downstream of FER and, probably, some FER homologs.

Tip-Localized RALF1-FER Facilitates eIF4E1 Polar Localization and Protein Synthesis

We then analyzed the localization of FER (*pFER::FER-GFP*) (Kessler et al., 2010; Du et al., 2016) and RALF1 (*pRALF1::RALF1-GFP*) in developing RHs at several growth stages. The clear polar localization of both of the encoded fusion proteins during the pre-initiation, initiation, and rapid growth stages of RH development (Figure 6E and 6F) decreased and disappeared as RH elongation was completed (Figure 6E and 6F). Similarly, eIF4E1 showed polar localization in RHs at the same three stages (Figure 6G). Next, we investigated eIF4E1 localization in *fer-4* and *fer-5*. In both *fer* mutants, eIF4E1 localized at the basal ends of trichoblasts (root epidermal cells responsible for RH development; Figure 6H), indicating that eIF4E1 requires FER for correct localization. We observed this phenomenon in *fer* mutant roots at the growth stage, where eIF4E1 was diffusely distributed in the cytoplasm rather than localized in the apical region (Figure 6H). These results imply that FER affects the polar localization of eIF4E1 by recruiting and interacting with eIF4E1 at the PM.

To verify that RALF1–FER mediates eIF4E1 polar localization, we examined the subcellular localization of eIF4E1-GFP, eIF4E1^{mutA}-GFP in WT and *fer-4* RH cells with or without RALF1 treatment (Supplemental Figure 12A–12C). RALF1 induced the detachment of eIF4E1 from its polar location in two early initiation phases in RH cells after 30 min (Supplemental Figure 12A). However, the visualization of the localization of eIF4E1^{mutA}-GFP and eIF4E1-GFP in *fer-4* revealed no obvious polar localization with or without RALF1 treatment (Supplemental Figure 12B and 12C). A more detailed time-series immune detection assay further confirmed these results (Figure 6I). Therefore, these data confirm that RALF1–FER regulates eIF4E1 polar localization.

ROP2 functions in cell morphogenesis and exhibits polar localization similar to that of the FER–eIF4E1 module (Molendijk et al., 2001); previous protein level, RIP, and polysome profiling assays indicated that ROP2 protein synthesis is regulated by RALF1–FER–eIF4E1 (Figures 2 and 5H and Supplemental Figures 1E, 2, 3, and 7D). Therefore, we investigated the polar localization of ROP2 in the RHs of *fer* and *4e/iso* mutants. Whereas ROP2 shows polar localization in the WT (Molendijk et al., 2001; Nibau et al., 2006) (Supplemental Figure 12D), it localized to the basal ends of RHs in *fer-4* (Supplemental Figure 12D). In the *fer-5* background, the polar localization of ROP2 was lost at the tip growth stage (Supplemental Figure 12D). These results indicate that the *FER* mutation affects ROP2 localization during polar RH growth. In addition, the *4e/iso* mutations affected tip-localized ROP2 accumulation, and the polar localization of ROP2 was lost more frequently in *4e/iso* than in the WT (Supplemental Figure 12E). Furthermore, the formation of the FER–ROP2 complex mediated by the FER–GEF1/4/10/14 interaction (Duan et al., 2010) was unaltered in the *4e/iso* mutant, implying that the reduced FER-based recruitment of ROP2 does not cause the defects in ROP2 accumulation observed in the *4e/iso* mutant (Supplemental Figure 12F). ROP2 still showed polar localization in *gef1/4/10/14* mutants, indicating that, in addition to the recruitment of ROP2 by the FER–GEF1/4/10/14 module, other mechanisms (e.g., local protein synthesis) that maintain ROP2's polar localization likely exist (Supplemental Figure 12G). Based on these observations, we propose that the spatially precise accumulation of ROP2 is partly dependent on protein synthesis via the RH tip-localized RALF1–FER–eIF4E1 module.

RSL4 Directly Suppresses *RALF1* Expression to Form a Feedback Regulatory Loop

Finally, we examined whether negative feedback may control the RALF1–FER pathway in RH cells. We first observed that RALF1 treatment reduced endogenous *RALF1* expression in the WT after 50 min (Figure 7A). In addition, RSL4-OE reduced *RALF1* mRNA levels (Figure 7A), whereas a mutant lacking RSL4 and the related protein RSL2 (*rsl4/rsl2*) (Yi et al., 2010) showed upregulation of *RALF1* expression (Figure 7A), indicating that RSL4 may regulate *RALF1* expression. We next tested whether the RSL4 transcription factor could bind to the *RALF1* promoter. RSL4 can specifically bind and control the expression of RH-SPECIFIC (RHS) genes, which contain an RH-specific *cis*-element (RHE) in their regulatory region (Hwang et al., 2017). We found that the *RALF1* promoter contained a

Please cite this article in press as: Zhu et al., The RALF1–FERONIA Complex Phosphorylates eIF4E1 to Promote Protein Synthesis and Polar Root Hair Growth, Molecular Plant (2019), https://doi.org/10.1016/j.molp.2019.12.014

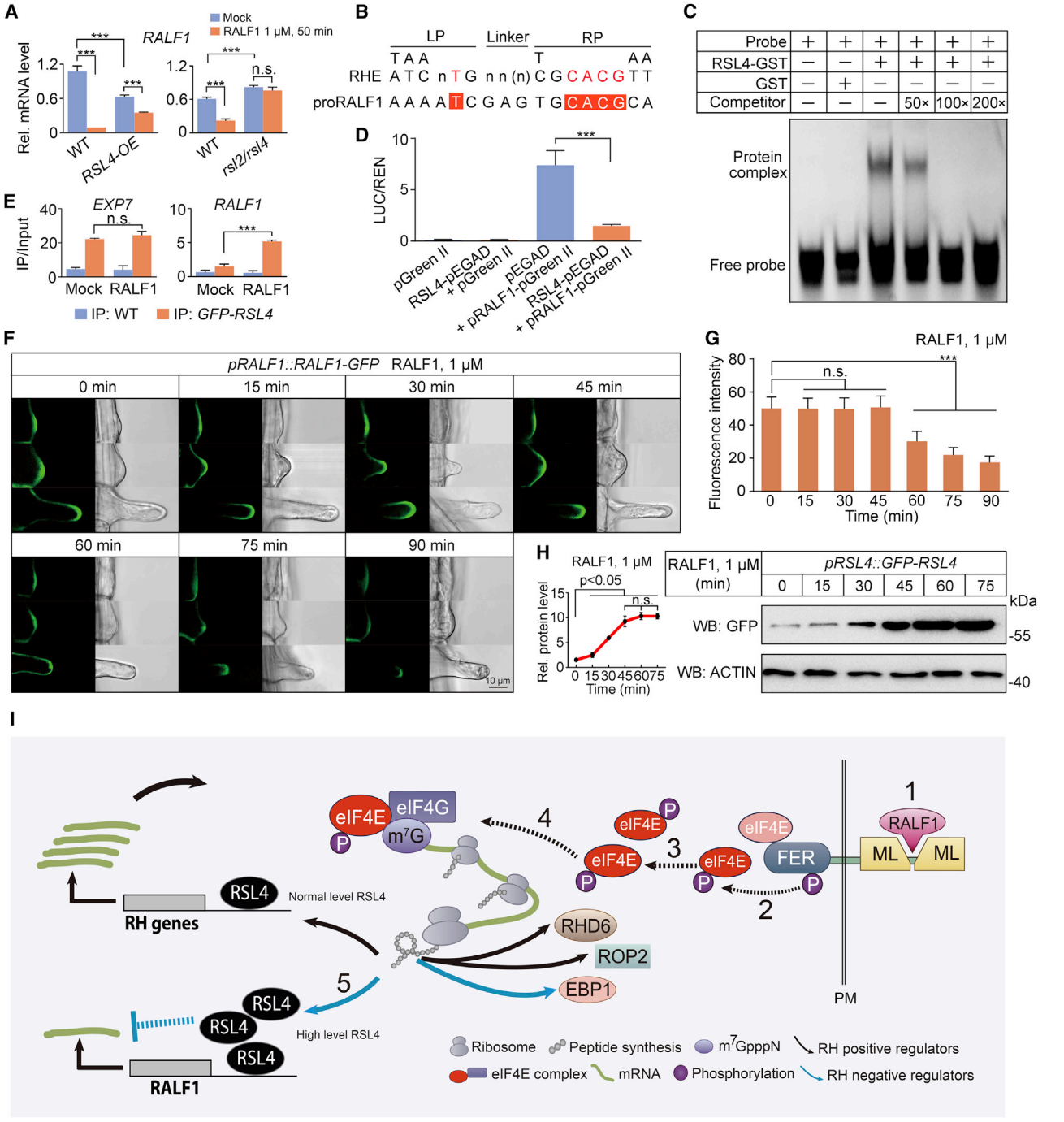

Figure 7. RSL4 Suppresses the Expression of *RALF1* by Directly Binding Its Promoter.

(A) RT-qPCR analysis of *RALF1* expression with or without RALF1 treatment.

(B) RHE structure (top), with LP, RP, and linker sequences; *RALF1* RHE consensus sequences of (bottom).

(C) EMSA showing RSL4 binding to the proRALF1 RHE.

(D) Dual-LUC assay.

(E) GFP-RSL4 ChIP assay.

(F) Fluorescence intensity of RALF1-GFP with or without RALF1 treatment.

(G) Quantification of the fluorescence intensity at different time points in **(F)** (30 RH cells from seven to nine growing roots).

(H) Protein accumulation of GFP-RSL4 after RALF1 treatment. The relative protein level of RSL4 was analyzed using ImageJ.

(I) Model of polar RH growth controlled by the autocrine RALF1–FER–eIF4E–RSL4 pathway. The numbers 1–5 in this model show the main steps: (1) RALF1 binding to FER; (2) eIF4E recruitment and phosphorylation by FER; (3) dissociation of phosphorylated eIF4E from FER; (4) phosphorylated eIF4E cap binding and increased protein translation; (5) repression of *RALF1* expression by high levels of RSL4. Data are shown as the mean ± SD; ***$p < 0.001$; n.s., non-significant by one-way ANOVA.

Please cite this article in press as: Zhu et al., The RALF1–FERONIA Complex Phosphorylates eIF4E1 to Promote Protein Synthesis and Polar Root Hair Growth, Molecular Plant (2019), https://doi.org/10.1016/j.molp.2019.12.014

DNA sequence with a typical RHE (Figure 7B) and that RSL4 indeed bound to the RHE sequence *in vitro* in an electrophoretic mobility shift assay (EMSA) (Figure 7C). Using a dual-luciferase (LUC) assay, we confirmed that RSL4 suppressed *RALF1* transcription in an *Arabidopsis* protoplast system (Figure 7D), further suggesting that RSL4 binds *RALF1 in vivo*. Finally, we confirmed this result *in vivo* using a chromatin IP (ChIP)–qPCR assay with or without RALF1 peptide treatment (Figure 7E). RSL4 bound the *EXP7* (Hwang et al., 2017) promoter regardless of RALF1 treatment, but the association between the RSL4 protein and the enrichment of RHE sequences in the *RALF1* promoter is RALF1 dependent (Figure 7E). Because RALF1–FER promotes RSL4 protein synthesis, these data suggest that only when the expression of the RSL4 protein reaches a high level will it bind to the *RALF1* promoter and inhibit *RALF1* expression. To further test this possibility, we observed *pRALF1::RALF1-GFP* fluorescence and found that it was reduced 60 min after RALF1 administration (Figure 7F and 7G), whereas RSL4 peaked 45 min after RALF1 administration (Figure 7H), indicating that after the RSL4 level peaks, *RALF1* expression starts to decline. Taken together, these findings reveal a negative feedback loop in which, after RSL4 levels are upregulated via the RALF1–FER pathway, high levels of RSL4 suppress *RALF1* mRNA expression by directly binding to the *RALF1* promoter, thus negatively affecting the RALF1–FER signaling pathway.

DISCUSSION

The molecular links between extracellular signals and the regulation of localized protein synthesis in plant cells are largely unclear. Our results show that an extracellular peptide, RALF1, and its receptor, FER, regulate protein synthesis by activating eIF4E1 in a spatiotemporally precise manner to determine the final size of RH cells (Figure 7I). We propose that RHs use this autocrine RALF1–FER–eIF4E1-mediated pathway to explore the availability of nutrients, water, and microorganisms in the soil environment. It is unknown how RALF1–FER–eIF4Es achieve the translation of specific subsets of mRNAs to provide an additional layer of complexity in the diverse contexts of plant growth and development (Li et al., 2016; Liao et al., 2017; Franck et al., 2018). One strategy might include ribosomal heterogeneity, which involves selective functional ribosomal subpopulations that exhibit variation in their RNA or protein components and modulate the translational program in response to environmental changes. Receptors may work together with distinct ribosomal subpopulations to fulfill various roles. In *Caenorhabditis elegans*, IFE-1 affects the expression of sperm-specific proteins (Henderson et al., 2009). In *Drosophila melanogaster*, eIF4E-3 is a testis-specific protein required only for spermatogenesis (Hernández et al., 2012; Ghosh and Lasko, 2015), and 4EHP is a translational repressor that inhibits the translation of specific mRNAs during early embryogenesis (Yarunin et al., 2011). Some recent studies have indicated that under conditions of extreme oxygen depletion (hypoxia), human cells exhibit an alternative cap-dependent translation process involving 4EHP (Uniacke et al., 2012; Timpano and Uniacke, 2016) and that eIF4E-3 acts as a tissue-specific tumor suppressor (Osborne et al., 2013). Here, we showed that FER can interact with eIF4E1, eIF(iso)4E, eIF4E1b, and eIF4E1c. Therefore, FER can recruit different eIF4E proteins to form distinct ribosomal subpopulations that control the translation of specific sets of mRNAs and fulfill various roles. Another strategy could be related to RLK interactions with different RNA-binding proteins to regulate multiple responses (Nicaise et al., 2013; Kim et al., 2015). The regulation of gene-specific translation always involves the direct interaction of an RNA-binding protein with specific 3′ untranslated region sequences and the subsequent recruitment of polysomes (Szostak and Gebauer, 2012). We found that the lack of FER in *fer-4* caused the appearance of an extra 60S peak between the 40S and the 80S peaks in polysome profiling assays and a decrease in the intensity of polysomal fractions, indicating that *fer-4* shows greatly altered ribosome-mediated protein synthesis. Whether FER uses other mechanisms to regulate protein synthesis is still an open question.

In RH cells, RALF1–FER–eIF4Es upregulate the translation of a subset of key proteins (e.g., RHD6, RSL4, and ROP2) that sustain polar RH growth. As observed under RALF1 treatment, the accumulation of certain newly synthesized proteins such as EBP1 (a negative regulator of RH size) (Li et al., 2018), as well as the inhibition of *RALF1* expression by high RSL4 expression, may exert negative feedback on RALF1 signaling, thereby stopping RH growth. We hypothesized that the RALF1–FER–eIF4E pathway determines the final cell size by modulating protein synthesis in response to changes in environmental cues under both normal and stress conditions (e.g., salt, drought, and pathogen invasion) (Kessler et al., 2010; Szostak and Gebauer, 2012; Chen et al., 2016; Stegmann et al., 2017; Feng et al., 2018). Further investigations will elucidate how each eIF4E protein is able to regulate specific protein translation programs that control specific cellular processes in a cell-type-specific manner.

METHODS

Plant Materials and Growth Conditions

A. thaliana seeds were surface sterilized and, unless stated otherwise, stratified at 4°C for 2 d before being grown on $^1/_2$-strength Murashige and Skoog medium (1/2 MS) with 0.8% sucrose and 1% Phytagel (Sigma-Aldrich) for subsequent analysis. WT (Col-0), *fer-4* (Duan et al., 2010), *fer4/gFER-K565R* (Haruta et al., 2018), *gef1/4/10* (Yu et al., 2012), *ralf1-1* (Salk_036331) (Du et al., 2016), *Ubi::FER-FLAG* (Du et al., 2016), *pFER::FER-GFP* (Yu et al., 2014), *pRSL4::GFP-RSL4* (Datta et al., 2015), and *35S::RSL4 (RSL4-OE)* (Mangano et al., 2017) plants were previously described. For overexpression assays, full-length *eIF3G* and *eIF4E1* coding sequences fused with a C-terminal MYC tag driven by the *ACT2* promoter were cloned into pDT1. For generating transgenic plants carrying the point mutant constructs *35S::eIF4E1^{mutA}-GFP* and *35S::eIF4E1^{mutD}-GFP* (phosphorylation-site mutant), the *eif4e1* mutant was transformed with vectors *eIF4E1^{mutA}-2300GFP* and *eIF4E1^{mutD}-2300GFP*. In T_2 transgenic plants, the *eif4e1* background was genotyped by PCR using specific primers (Supplemental Table 1). We replaced the *Ubi* promoter with *pEXP7* to generate the *pEXP7::FER-FLAG* construct. The full-length *EBP1* coding sequence fused with a FLAG tag driven by the *Ubi* promoter was cloned into pCAMBIA1301. The *eif4e1 eif(iso)4e* double mutant was obtained by crossing *eif4e1* (Salk_067430) with *eif(iso)4e* (Salkseq_059591.1) and then confirmed by PCR with specific primers (Supplemental Table 1). We further obtained the triple mutant *eif4e1 eif(iso)4e eif4e1b* (*4e/iso/4eb*) via CRISPR-Cas9 knockout of the *eIF4e1b* (At1g29550) gene in a *4e/iso* background; the mutant target was amplified by PCR using gene-specific primers (Supplemental Table 1) and sequenced. The *eIF4E1/fer-4*, *eIF4E1^{mutA}/fer-4*, and *eIF4E1^{mutD}/fer-4* materials were obtained by crossing the *35S::eIF4E1-GFP*, *35S::eIF4E1^{mutA}-GFP*, and *35S::eIF4E1^{mutD}-GFP* plants with *fer-4*. In

Please cite this article in press as: Zhu et al., The RALF1–FERONIA Complex Phosphorylates eIF4E1 to Promote Protein Synthesis and Polar Root Hair Growth, Molecular Plant (2019), https://doi.org/10.1016/j.molp.2019.12.014

the F_2 generation, the *fer-4* background was genotyped by PCR using gene-specific primers (Supplemental Table 1) (Duan et al., 2010). WT, mutants, and transgenic lines were grown at 23°C with a photoperiod of 16 h light/8 h dark. Typically, 4-day-old plants were used for RH pictures and statistical analysis, and 8-day-old plants were harvested for western blot, RIP assays, and polysome profiling analyses unless specifically mentioned.

Statistical Analysis

SPSS Statistics 17.0 software was used here. Data are shown as mean ± SD; $*p < 0.05$, $**p < 0.01$, $***p < 0.001$, n.s., no significance, by one-way ANOVA, least significant difference.

Phenotypic Analysis

For the root length measurements, seeds of different genotypes were germinated for 4 days on 1/2 MS and then RHs approximately 0.6–0.8 mm from the root tip were measured with an Olympus SZX16 stereomicroscope. RH length was measured from the digital images using ImageJ software 1.52e. Measurements for at least eight seedlings (n = 8, 80–200 RHs) of each genotype were recorded. For RALF1 treatments, 2-day-old vertically grown *A. thaliana* seedlings were carefully transferred to filter papers that were soaked with 1/2 MS liquid culture medium containing different RALF1 and CHX concentration combinations. We performed CHX treatment for a shorter time twice (4 h/day) within 2 days to block protein synthesis, and we obtained similar results. The seedlings were incubated for 2 d followed by RH measurements and statistical analysis. RH growth rate was imaged by capturing time-lapse images at 5 min intervals with an Olympus SZX16 stereomicroscope. Images were collected for a total of 1 h, and root lengths were measured using ImageJ software to determine the growth rate. The RALF1-mediated primary root growth inhibition was analyzed as previously described (Haruta et al., 2014).

Microscopy Imaging

Confocal images of the pFER::FER-GFP polar localization in RHs were obtained on a Zeiss confocal laser scanning microscope using a 488 nm band-pass filter (laser, 7%; detector gain, 675.2; detector offset, −10). A Nikon confocal laser scanning microscope with a 488 nm band-pass filter was used for detection of GFP-RSL4 produced from the *pRSL4::GFP-RSL4* construct (laser power, 1.0; PMT HV, 170; offset, −127), eIF4E1-GFP (eIF4E1^{mutA}-GFP) produced from the *35S::eIF4E1-GFP* (*35S::eIF4E1^{mutA}-GFP*) construct (laser power, 2.0; PMT HV, 136; offset, −127), *pROP2::ROP2-GFP* fluorescence intensity in roots (laser power, 1.0; PMT HV, 117; offset, −127), and RHs (laser power, 1.0; PMT HV, 127; offset, −127) with or without RALF1 treatment, pRALF1::RALF1-GFP polar localization in RHs (laser power, 1.0; PMT HV, 117; offset, −127), and fluorescence intensity in RHs with or without RALF1 treatment (laser power, 1.0; PMT HV, 133; offset, −127). For FRAP experiments (Datta et al., 2015), bleaching was performed by raising the intensity of the 488 laser to 100%. This was repeated until complete bleaching of fluorescence was observed. Fluorescence was bleached in less than 2 min. Recovery of the fluorescence was recorded at 5 and 10 min after bleaching. Ten to fifteen nuclei at each of the RH growth stages were bleached. Quantification of the fluorescence intensity was carried out with ImageJ software.

Protein Level Assay

To avoid the manipulation of the seedlings during the transfer from solid to liquid medium for RALF1 treatment, seedlings were first removed from the solid medium. After agar was removed, the seedlings were transferred into liquid 1/2 MS medium to pre-incubate for 1 h before treatment. The seedlings were then soaked with RALF1 (in 1/2 MS liquid medium) or mock control (1/2 MS medium containing protein elution buffer used for RALF1 purification). We confirmed that pre-incubation for 1 h before treatment can avoid the detection of changes in protein levels that may have been caused by removal from the solid medium. After germination for 8 days, seedlings (around 100 mg) were treated with RALF1 (1 μM), RALF1 (1 μM) + CHX (14 μM), or RALF1 (1 μM) + CRD (50 μg/ml) for the indicated times and then pulverized in liquid nitrogen. The pulverized samples were suspended in 100 μl buffer (40 mM Tris–HCl [pH 7.5], 100 mM NaCl, 1 mM EDTA, 5% glycerol, 0.75% Triton X-100, 1 mM PMSF, and 1% proteinase inhibitor mixture [Thermo Fisher Scientific, 78420]) and centrifuged for 15 min at 16 000 *g* at 4°C. Around 40 μl of each sample was used for SDS–PAGE to determine protein concentrations. The samples from different time points or different treatments were run on the same gel. The different proteins for analysis were separated on the same gel and probed with ROP2 antibody (Abiocode, Q38919), EBP1 antibody (Li et al., 2018), FLAG antibody (Abmart, M20008), GFP antibody (CMC TAG, AT0028), and ACTIN antibody (Abmart, M20009) after cutting off the polyvinylidene fluoride membrane. ACTIN was used as the internal control for protein input. Quantification of protein levels was carried out using ImageJ.

Polysome Profiling Assay and Real-Time PCR

Arabidopsis polysomes were fractionated over sucrose gradients as described (Missra and von Arnim, 2014), with minor modifications. Sucrose gradients (15%–60%) were prepared by layering 3.3 ml of 15% sucrose on top of an equal volume of 60% sucrose in 38 ml polycarbonate centrifuge tubes (Beckman Coulter). Gradients were stored at −80°C until the day before using. They were moved to a cold room to gradually thaw overnight and form a continuous density gradient before being subjected to centrifugation. To avoid the manipulation of the seedlings during the transfer from solid to liquid medium for RALF1 treatment, seedlings were transferred into liquid 1/2 MS medium to pre-incubate for 1 h before treatment. Then, 8-day-old seedlings (around 500 mg) were treated with RALF1 (1 μM) and CRD (150 μg/ml) for 30 min. For harvesting, samples were ground in liquid nitrogen with a mortar and pestle and then resuspended in 1 ml of extraction buffer (0.2 M Tris–HCl [pH 7.5], 50 mM KCl, 25 mM $MgCl_2$, 1% deoxycholic acid, 50 μg/ml CHX, and 400 U/ml RNase inhibitor [Promega]). After being spun for 15 min at 4°C, 800 μl of supernatant was loaded onto a 36 ml continuous sucrose gradient (15%–60%) in a polycarbonate tube and spun in a Beckman SW 32 Ti rotor at 17 000 *g* for 4 h at 4°C. Then, 80 μl of supernatant was saved as input, and total mRNA was isolated from this sample with the RNeasy Plant Mini Kit (Qiagen). We collected 11 fractions by carefully pipetting 3 ml samples from the top of the gradient. The polysomal and non-polysomal fractions were determined based on UV absorption profiles obtained from identical but separate experiments. Under our conditions, the top seven fractions (1–7) contained ribosome-free mRNAs and monosomes and the bottom four fractions (8–11) contained mRNAs associated with multiple ribosomes. Then, the bottom four fractions were mixed with the same volume of RNAiso plus (Takara) and RNA was isolated. For RT-qPCR analysis, we quantified the relative content of the total target transcripts in the input and the relative content of target transcripts associated with heavier polysomes in the bottom four fractions. Then we calculated the relative proportion of the target transcripts associated with heavier polysomes in the total mRNA. We used *ACTIN* as the reference gene. For *ACTIN*, we used *eIF4A* as the reference gene. Primers for RT-qPCR are shown in Supplemental Table 1.

Bioinformatic Analysis

The gene expression levels were analyzed in ePlant (http://bar.utoronto.ca/eplant/) (Waese et al., 2017). A heatmap was made with Morpheus (https://software.broadinstitute.org/morpheus/). Cluster analysis was also performed with Morpheus using the Euclidean distance metric.

Yeast Two-Hybrid Assay

Y2H assays were performed as previously described (Chen et al., 2016; Du et al., 2016; Stegmann et al., 2017). Briefly, the coding sequences of *eIF4Es* were cloned into pGADT7 (AD). Primers for cloning are shown in Supplemental Table 1. The kinase domain of FER was cloned into pGBKT7 (BD). Distinct plasmid pairs were transformed into yeast AH109 cells. The transformants were diluted and plated onto synthetic dropout

Please cite this article in press as: Zhu et al., The RALF1–FERONIA Complex Phosphorylates eIF4E1 to Promote Protein Synthesis and Polar Root Hair Growth, Molecular Plant (2019), https://doi.org/10.1016/j.molp.2019.12.014

medium lacking tryptophan/leucine (+His) and synthetic dropout medium lacking tryptophan/leucine/histidine (−His) but supplemented with 20 mM 3-amino-1,2,4-triazole for 7 days to test the interaction.

GST Pull-Down Assay

Recombinant His-FER–CD protein was incubated overnight at 4°C with GST beads coupled with GST-eIF4E1 in binding buffer (20 mM HEPES [pH 7.5], 40 mM KCl, 5 mM $MgCl_2$). The beads were washed five times with TBS buffer (50 mM Tris [pH 7.5], 150 mM NaCl) and boiled in SDS–PAGE sample buffer, and eluted proteins were analyzed by immunoblotting with His antibody (Abmart, M20001) or GST antibody (CMC, SC-80998). We did the *in vitro* phosphorylation assays described as follows first, then used the phosphorylated protein to do the ATP-dependent GST pull-down assay. Samples were boiled in 1× SDS loading buffer for 5 min and separated on a 10% (m/v) SDS–PAGE gel, which was prepared with 60% glycerol, and the gel-shift time was properly extended to show the slight upward shifted band of phosphorylated protein.

Bimolecular Fluorescence Complementation Assay

For the BiFC assay, FER-nVenus and eIF4E1-cCFP were cloned into the pE3308 and pE3449 plasmids, respectively (Supplemental Table 1) (Du et al., 2016). Mesophyll protoplasts were isolated from well-expanded rosette leaves of 30-day-old *Arabidopsis* plants through cellulase and macerozyme digestion. Then, protoplasts were co-transfected with FER-nVenus and eIF4E1-cCFP constructs or negative control constructs using the polyethylene glycol transformation method as previously described (Du et al., 2016). The co-transfected protoplasts were incubated in the dark at 23°C for 18 h to allow expression of the BiFC proteins. Fluorescence was monitored with a confocal microscope using an excitation wavelength of 488 nm for GFP and 560 nm for FM4-64 dye (red).

Co-immunoprecipitation Assay

CoIP was performed as previously described with some modifications (Du et al., 2016; Li et al., 2018). Briefly, 8-day-old *Ubi::FER-FLAG* or *pEXP7::FER-FLAG* transgenic seedlings were first treated with or without 1 μM RALF1 in 1/2 MS liquid medium for the indicated times. These seedlings were ground to a fine powder in liquid nitrogen and solubilized with NEB-T buffer (1% Triton X-100, 20 mM HEPES [pH 7.5], 40 mM KCl, 1 mM EDTA, 1 mM PMSF, and 1% protease inhibitor). The mixture was then incubated for 1.5 h at 4°C, extracts were centrifuged at 16 000 *g* at 4°C for 20 min, and the supernatant was incubated with pre-washed anti-FLAG M2 agarose gel (Sigma-Aldrich, A2220) overnight at 4°C. The agarose gel was washed six times with NEB-T buffer and eluted with 3× FLAG peptide (Sigma-Aldrich, F4799) at 4°C for 5 h. FLAG antibody (Abmart, M20008) and eIF4E1 antibody (Abiocode, O23252) were used for the immunoblot assay. Samples were boiled in 1× SDS loading buffer for 5 min and separated on a 10% (m/v) SDS–PAGE gel, which was prepared with deionized water, and the gel-shift time was properly shortened to show total FER content (including phosphorylated and dephosphorylated forms) in one band.

In Vitro Phosphorylation Assay and Liquid Chromatography–Tandem Mass Spectrometry Analysis

Recombinant His-eIF4E1 (encoding eIF4E1 amino acids 1–236 fused with an N-terminal His tag) was generated using the pRSF vector (Li et al., 2018). The primers used for cloning are shown in Supplemental Table 1. Recombinant His-FER–CD and its kinase-dead form (His-FER^{K565R}–CD) were generated as previously described (Chen et al., 2016; Du et al., 2016). *In vitro* phosphorylation assays were performed as described previously with some modifications (Li et al., 2018): His-FER–CD and His-eIF4E1 (0.5 μg of each) were added to the kinase assay solution containing 25 mM Tris (pH 7.5), 10 mM $MgCl_2$, 1 mM $CaCl_2$, 1 mM DTT, and 1 mM ATP. After gentle mixing, the mixture was co-incubated for 30 min at 30°C. The reaction was stopped by adding 1× SDS loading buffer. The phosphorylated His-eIF4E1 was detected with a phospho-threonine antibody (pThr; Cell Signaling, 9381S). For analysis of the eIF4E1 phosphorylation sites, we used a co-expression system according to our previous work (Du et al., 2016). This co-expression system in *E. coli* was designed to examine the *in vivo* phosphorylation process (Du et al., 2016). For the phosphorylation assay, we constructed pACYC-PYL1-FER, pACYC-PYL1-FER^{K565R}, and pRSF-ABI1-eIF4E1. pRSF-ABI1-eIF4E1, together with pACYC-PYL1-FER (or pACYC-PYL1-FER^{K565R}), was transformed into BL21 *E. coli*. The transformed *E. coli* were inoculated into LB medium (containing kanamycin and chloromycetin) and cultured at 37°C until the OD_{600} reached 0.6. Then, 250 μM isopropyl-β-D-thiogalactoside was added to induce protein expression for 3 h before 50 μM ABA was added to the bacterial culture to release the FER phosphorylation activity for 20 min. After co-expression with FER–CD or FER^{K565R}–CD, His-eIF4E1 protein was purified and then subjected to alkylation/tryptic digestion followed by liquid chromatography–tandem mass spectrometry (LC-MS/MS) (Li et al., 2018). No phosphorylation site was detected in the FER^{K565R}−CD negative control. The FER-GFP interacting proteins identified via IP–MS/MS were described in our previous work (Mao et al., 2015), and fold-enrichment calculations were made for all identified peptides within a group (Mao et al., 2015).

Homology Modeling of Protein Structure

The cap-binding domain of *A. thaliana* eIF4E1 (S59-A235) was modeled through an iterative threading algorithm using the I-TASSER server (Roy et al., 2010). The estimated TM-score and C-score are 0.92 ± 0.06 and 1.49, respectively. Hence, this model appears to be acceptable. 7N-Methyl-8-hydroguanosine-5′-triphosphate (MGT; a cap analog) was modeled into the cap-binding site of AteIF4E1 by COFACTOR (Zhang et al., 2017) and COACH (Yang et al., 2013), using the *D. melanogaster* eIF4E–MGT complex (PDBID: 4UEC) as a template. The structure of the AteIF4E1–cap complex was generated using PyMOL (DeLano, 2002).

In Vivo Phosphorylation Assay

About 1.5 g of 8-day-old seedlings (WT, *eIF4E-GFP-1*, *eIF4E^{mutA}-GFP-1*, and *eIF4E-1/fer-4*) was treated with or without RALF1 (1 μM) peptide for 30 min. Samples were ground to a fine powder in liquid nitrogen and solubilized with 600 μl NEB-T buffer (20 mM HEPES [pH 7.5], 40 mM KCl, 1 mM EDTA, 1% Triton X-100, 1 mM PMSF, 1% protease inhibitor mixture [Thermo Fisher Scientific, 78420], and 1% phosphatase inhibitors [Bimake, B15001]). After incubation at 4°C for 1 h, the extracted samples were centrifuged at 16 000 *g* for 15 min to collect the supernatant. GFP-trap beads (Chromotek, gta-100, 20 μl per IP) were washed two times in NEB-T buffer and then the beads were used to immunoprecipitate eIF4E1-GFP or eIF4E^{mutA}-GFP protein complexes at 4°C for 5 h with end-over-end rotation. Beads were washed six times with wash buffer (20 mM HEPES [pH 7.5], 40 mM KCl, and 0.1% Triton X-100). Finally, 30 μl of elution buffer (20 mM HEPES [pH 7.5] and 40 mM KCl) was added. Samples were boiled in 1× SDS loading buffer for 5 min. In order to get a very clear picture, we divided the sample equally into two tubes (15 μl/tube) and separated them on two 8% (m/v) SDS–PAGE gels, which were prepared with deionized water; blots were probed with pThr antibody (Cell Signaling, 9381S) or GFP antibody (CMC, AT0028),. At least three biological replicates of this assay were performed, with similar results.

m^7GTP Pull-Down Assay

Recombinant GST-eIF4E1 (encoding eIF4E1 amino acids 1–236 fused with an N-terminal GST tag) was generated using the pEGX4T-1 vector. Primers for cloning are shown in Supplemental Table 1. Recombinant His-FER–CD and its kinase-dead form (His-FER^{K565R}–CD) were generated as previously described (Du et al., 2016; Li et al., 2018). *In vitro* phosphorylation assays were performed as described above. After the reaction, phosphorylated GST-peIF4E1 or non-phosphorylated GST-eIF4E1 was purified with GST Sepharose beads and was used in the next steps. m^7GTP pull-down assays were performed as described by Tomoo et al. (2002). Briefly, m^7GTP (1 μM) Sepharose beads (Jena Bioscience, AC-155S) were washed with 500 μl buffer A (20 mM

Please cite this article in press as: Zhu et al., The RALF1–FERONIA Complex Phosphorylates eIF4E1 to Promote Protein Synthesis and Polar Root Hair Growth, Molecular Plant (2019), https://doi.org/10.1016/j.molp.2019.12.014

HEPES–KOH [pH 7.5], 1 mM DTT, 0.1 mM EDTA, and 100 mM KCl) three times, added to 0.1 μM purified protein (pre-cleared with Sepharose resin without m^7GTP for 1 h), and rotated for the indicated times at 4°C. The beads were washed five times with buffer A. The samples were then denatured, and the supernatants were loaded onto SDS–PAGE for immunoblot analysis.

Fluorescence Titration Assay

The titration experiments (Niedzwiecka et al., 2002) were carried out on an F-7000 FL spectrophotometer at 20°C in a standard buffer containing 50 mM HEPES–KOH (pH 7.2), 100 mM KCl, 0.5 mM EDTA, and 1 mM DTT. For eIF4E1–cap association, both forms of eIF4E1 at a concentration of 0.1 μM in standard buffer were titrated with increasing concentrations of cap solution (Jena Bioscience, NU-1122S) (working concentration: 0–1 μM). Protein fluorescence was excited at 280 nm and observed at 337 nm.

RNA Immunoprecipitation Assay

Seedlings were germinated for 8 days and then about 1.5 g of seedlings was removed from the agar medium and transferred into liquid 1/2 MS medium to pre-incubate for 1 h before treatment. Then, seedlings were treated with or without RALF1 (1 μM) peptide for 30 min, immersed in 0.5% paraformaldehyde, and incubated under vacuum (0.1 MPa) for 10 min. Formaldehyde cross-linking was reversed by incubating samples in 2 M glycine for 4 min. Samples were washed three times with ddH_2O and then ground to a fine powder in liquid nitrogen and solubilized with 300 μl extraction buffer (20 mM Tris–HCl [pH 8.0], 5 mM EDTA, 1% Triton X-100, 0.05% SDS, 1 mM PMSF, 5 mM EGTA, 10 mM DTT, and 80 U RNase inhibitor). After incubation for 1 h at 4°C, the extracted samples were centrifuged at 16 000 *g* for 15 min to collect the supernatant. Samples were diluted 10-fold with dilution buffer (1% Triton X-100, 167 mM NaCl, 16.7 mM Tris–HCl [pH 8.0], 1.2 mM EDTA, and 80 U RNase inhibitor). Protein A/G magnetic beads (Bimake, B23202) (60 μl per IP) were washed three times in binding/washing buffer (150 mM NaCl, 20 mM Tris–HCl [pH 8.0], 2 mM EDTA, 1% Triton X-100, 0.1% SDS, 1 mM PMSF, and 80 U RNase inhibitor). Then, beads were incubated with eIF4E1 antibody or IgG control antibody at room temperature for at least 1 h with end-over-end rotation. Antibody-conjugated beads were washed three times using binding/washing buffer. Then, the beads were added to the previously prepared supernatant and mixed for 8 h at 4°C with end-over-end rotation. Beads were washed and then separated from washing buffer using a magnetic microcentrifuge tube rack. Beads were incubated for 30 min at 55°C in RIP elution buffer (100 mM Tris–HCl [pH 8.0], 100 mM EDTA, 1% SDS, 80 U RNase inhibitor, and 30 μg proteinase K). RNA was extracted from the output and input samples by adding 1 ml RNAiso plus (Takara). The eluted RNA was used to generate cDNA for RT-qPCR. In parallel, input samples were used for quantification. Primers for RT-qPCR are shown in Supplemental Table 1.

Cytology and Immunodetection Assay

Three-day-old *A. thaliana* seedlings were collected in a 24-well plate (5 seedlings per well) and then incubated for 13 min under vacuum (0.05 MPa) in 1× phosphate-buffered saline (PBS) containing 4% paraformaldehyde and 0.1% Triton X-100. Seedlings were washed gently three times (5 min for each wash) in 1× PBS and then the cell wall was digested in 2% Driselase (Sigma, D8037) in 1× PBS for 18 min at 37°C and washed five times with 1× PBS. The permeability of the seedlings was increased by incubating them in 3% IGEPAL CA-630 (Sigma, 18896) and 10% DMSO in 1× PBS for 18 min, and the seedlings were washed three times with 1× PBS. Seedlings were incubated in 2% bovine serum albumin (BSA) (Ameresco, 0332) in 1× PBS, which was used as a blocking solution, for 1 h. Seedlings were then incubated with primary eIF4E1 antibody, ROP2 antibody, and IgG control antibody (antibody diluted 1:600 in blocking solution) for 8 h at 4°C in the dark. The seedlings were washed three times in blocking solution. Fluorophore-labeled secondary antibody (IF555 goat–rabbit secondary antibody [Sungene Biotech, GR200G-37E]) diluted 1:600 in blocking solution was incubated with the samples at 37°C for 5 h in the dark. Seedlings were washed five times with 1× PBS, stored at 4°C, and prepared for observation within 3 days. Fluorescent signal detection and documentation were performed using a Nikon confocal laser scanning microscope with a 560-nm band-pass filter for IF555 detection (laser power, 0.5; PMT HV, 67; offset, −127).

Electrophoretic Mobility Shift Assay

The EMSA was performed as described by Liu et al. (2008), with some modified steps. RSL4-GST protein and GST protein were used for the EMSA. The primer sequences were synthesized and labeled with a fluorescein isothiocyanate (FITC) fluorescent probe (TsingKe Biological Technology) (Supplemental Table 1). The DNA–RSL4 binding reaction contained 100 pg probe, 100 ng RSL4-GST protein, 10 mM Tris (pH 7.5), 5% glycerol, 1 mM $MgCl_2$, 50 mM KCl, 0.2 mg/mL BSA, 0.5 mM DTT, 0.5 mg/mL polyglutamate, and the indicated amount of unlabeled competitor. The reactions were incubated at room temperature for 20 min and fractioned by electrophoresis in a 6% native polyacrylaminde gel (acrylaminde:bisacrylamide, 29:1) containing 10% glycerol, 89 mM Tris (pH 8.0), 89 mM boric acid, and 2 mM EDTA. The FITC signal was detected using a fluorescence imager plate.

Dual-Luciferase Assay

The dual-LUC assay was performed as described by Liu et al. (2008), with modified steps. The *RALF1* promoter was cloned into the pGreen-0800-LUC vector as the reporter plasmid (pRALF1-pGreen II). The effector plasmid 35S::RSL4 was constructed using the pEGAD vector (RSL4-pEGAD). The reporter plasmid and effector plasmid were transferred into *Arabidopsis* protoplasts simultaneously as described above for the BiFC assay. Samples were incubated in the dark at 23°C (16 h) for the dual-LUC assay using the Dual Luciferase Reporter Gene Assay Kit (RG027, Beyotime). The LUC and REN signals were detected using a Modulus microplate multimode reader (Turner Biosystem). Three biological repeats were measured for each sample, and similar results were obtained.

Chromatin Immunoprecipitation Assay

The ChIP assay was performed as described by Liu et al. (2008). To avoid manipulation-related effects during plant transfer from solid to liquid medium, we transferred the seedlings into liquid 1/2 MS medium and pre-incubated them for 12 h. Then, seedlings were soaked with 1 μM RALF1 (included in the 1/2 MS liquid medium) or mock control (1/2 MS medium containing protein elution buffer, which was used for RALF1 purification) for 2 h and then treated with 1% formaldehyde under vacuum for 15 min at room temperature. Glycine was added to a final concentration of 0.125 M to stop cross-linking. The seedlings were washed twice with sterile water, frozen in liquid nitrogen, ground to a fine powder, and homogenized in the nuclear extraction buffer 1 (10 mM Tris–HCL [pH 8.0], 0.4 M sucrose, 10 mM $MgCl_2$, 0.1 mM PMSF, and protease inhibitor [Thermo Fisher Scientific, 78430]). Nuclei were precipitated by centrifugation in a centrifuge at 4,000 g for 20 min, washed with nuclear extraction buffer 2 (10 mM Tris–HCl [pH 8.0], 0.25 M sucrose, 10 mM $MgCl_2$, 1% Triton X-100, 0.1 mM PMSF, and protease inhibitor), and lysed in the nucleus lysis buffer (50 mM Tris–HCl [pH 8.0], 10 mM EDTA, 1% SDS, 0.1 mM PMSF, and protease inhibitor). Chromatin was sheared by sonication to approximately 500 bp. The chromatin solution was diluted 10-fold with ChIP dilution buffer (16.7 mM Tris–HCl [pH 8.0], 167 mM NaCl, 1.1% Triton X-100, 1.2 mM EDTA, 0.1 mM PMSF, and protease inhibitor). GFP-trap beads (Chromotek, gta-100, 30 μl per IP) were washed with ChIP dilution buffer two times and then mixed with the chromatin solution and incubated at 4°C overnight. Immunocomplexes were precipitated and washed with four different buffers: low-salt buffer (20 mM Tris–HCl [pH 8.0], 150 mM NaCl, 0.2% SDS, 0.5% Triton X-100, 2 mM EDTA), high-salt buffer (20 mM Tris–HCl [pH 8.0], 500 mM NaCl, 0.2% SDS, 0.5% Triton X-100, 2 mM EDTA), LiCl washing buffer (20 mM Tris–HCl [pH 8.0], 0.25 M LiCl, 1% NP-40, 1% sodium deoxycholate, 1 mM EDTA),

Please cite this article in press as: Zhu et al., The RALF1–FERONIA Complex Phosphorylates eIF4E1 to Promote Protein Synthesis and Polar Root Hair Growth, Molecular Plant (2019), https://doi.org/10.1016/j.molp.2019.12.014

and TE washing buffer (10 mM Tris–HCl [pH 8.0], 1 mM EDTA). The bound chromatin fragments were eluted with the elution buffer (50 mM Tris–HCl [pH 8.0], 10 mM EDTA, 1% SDS), and the cross-links were reversed by incubating at 65°C overnight. The mixture was treated with Proteinase K for 1 h at 45°C to remove proteins. DNA was extracted with phenol/chloroform/isoamyl alcohol and precipitated with a two-fold volume of 100% ethanol at −80°C for 4 h. To recover the DNA, the sample was spun at 16 000 rpm for 20 min at 4°C. The pellet was dried briefly and resuspended in 25 μl of TE buffer for further real-time PCR analysis.

SUPPLEMENTAL INFORMATION

Supplemental Information is available at *Molecular Plant Online*.

FUNDING

This work was supported by grants from the National Natural Science Foundation of China (NSFC-31400232, 31871396, 31571444), Young Elite Scientist Sponsorship program of CAST (YESS20160001), and the Open Research Fund of the State Key Laboratory of Hybrid Rice (Hunan Hybrid Rice Research Center) to F.Y. and from ANPCyT (PICT2016-0132 and PICT2017-0066) and ICGEB (CRP/ARG16-03) and Instituto Milenio iBio–Iniciativa Científica Milenio MINECON to J.M.E.

AUTHOR CONTRIBUTIONS

F.Y. conceived the project and designed the research; S.R.Z., H.D.L., Y.H.Z., T.Y., L.L., C.Y.L., C.Y.T., Y.C.W., and J.M.P. performed the research; X.M.L., J.M.E., and H.W.G. contributed new reagents/analytic tools; F.Y., J.M.E., and S.R.Z. analyzed data and wrote the paper; all authors reviewed and approved the manuscript for publication.

ACKNOWLEDGMENTS

We thank Dr. Alice Y. Cheung, Liam Dolan, Hyung-Taeg Cho, and Zixing Li for providing plant materials and Jorge P. Muschietti for critical comments and suggestions. No conflict of interest declared.

Received: September 8, 2019
Revised: December 7, 2019
Accepted: December 31, 2019
Published: January 3, 2020

REFERENCES

Avdulov, S., Li, S., Michalek, V., Burrichter, D., Peterson, M., Perlman, D.M., Manivel, J.C., Sonenberg, N., Yee, D., Bitterman, P.B., et al. (2004). Activation of translation complex eIF4F is essential for the genesis and maintenance of the malignant phenotype in human mammary epithelial cells. Cancer Cell **5**:553–563.

Bastet, A., Zafirov, D., Giovinazzo, N., Guyon-Debast, A., Nogué, F., Robaglia, C., and Gallois, J.L. (2019). Mimicking natural polymorphism in eIF4E by CRISPR-Cas9 base editing is associated with resistance to potyviruses. Plant Biotechnol J **17**:1736–1750.

Carol, R., Takeda, S., Linstead, P., Durrant, C., Kakesova, H., Derbyshire, P., Drea, S., Zarsky, V., and Dolan, L. (2005). A RhoGDP dissociation inhibitor spatially regulates growth in root hair cells. Nature **438**:1013–1016.

Chen, J., Yu, F., Liu, Y., Du, C., Li, X., Zhu, S., Wang, X., Lan, W., Rodriguez, P.L., Liu, X., et al. (2016). FERONIA interacts with ABI2-type phosphatases to facilitate signaling cross-talk between abscisic acid and RALF peptide in *Arabidopsis*. Proc. Natl. Acad. Sci. U S A **113**:E5519–E5527.

Cho, H., and Cosgrove, D. (2002). Regulation of root hair initiation and expansin gene expression in *Arabidopsis*. Plant Cell. **14**:3237–3253.

Datta, S., Kim, C., Pernas, M., Pires, N., Proust, H., Tam, T., Vijayakumar, P., and Dolan, L. (2011). Root hairs: development, growth and evolution at the plant-soil interface. Plant Soil **346**:1–14.

Datta, S., Prescott, H., and Dolan, L. (2015). Intensity of a pulse of RSL4 transcription factor synthesis determines *Arabidopsis* root hair cell size. Nat. Plants **138**:1–6.

DeLano, W. (2002). The PyMOL Molecular Graphics System (San Carlos, CA: Delano Scientific).

Drubin, D., and Nelson, W. (1996). Origins of cell polarity. Cell **84**:335–344.

Du, C., Li, X., Chen, J., Chen, W., Li, B., Li, C., Wang, L., Li, J., Zhao, X., Lin, J., et al. (2016). Receptor kinase complex transmits RALF peptide signal to inhibit root growth in *Arabidopsis*. Proc. Natl. Acad. Sci. U S A **113**:E8326–E8334.

Duan, Q., Kita, D., Li, C., Cheung, A.Y., and Wu, H.M. (2010). FERONIA receptor-like kinase regulates RHO GTPase signaling of root hair development. Proc. Natl. Acad. Sci. U S A **107**:17821–17826.

Dünser, K., Herger, A., Feraru, M.I., Ringli, C., and Kleine-Vehn, J. (2019). Extracellular matrix sensing by FERONIA and Leucine-Rich Repeat Extensins controls vacuolar expansion during cellular elongation in *Arabidopsis thaliana*. EMBO J. **38**:e100353.

Escobar-Restrepo, J.M., Huck, N., Kessler, S., Gagliardini, V., Gheyselinck, J., Yang, W.C., and Grossniklaus, U. (2007). The FERONIA receptor-like kinase mediates male-female interactions during pollen tube reception. Science **317**:656–660.

Etienne-Manneville, S., and Hall, A. (2002). Rho GTPases in cell biology. Nature **420**:629–635.

Favery, B., Ryan, E., Foreman, J., Linstead, P., Boudonck, K., Steer, M., Shaw, P., and Dolan, L. (2001). KOJAK encodes a cellulose synthase-like protein required for root hair cell morphogenesis in *Arabidopsis*. Genes Dev. **15**:79–89.

Feng, W., Kita, D., Peaucelle, A., Cartwright, H., Doan, V., Duan, Q., Liu, M.C., Maman, J., Steinhorst, L., Schmitz-Thom, I., et al. (2018). The FERONIA receptor kinase maintains cell wall integrity during salt stress through Ca^{2+} signaling. Curr. Biol. **28**:666–675.

Franck, C., Westermann, J., and Boisson-Dernier, A. (2018). Plant malectin-like receptor kinases: from cell wall to immunity and beyond. Annu. Rev. Plant Biol. **69**:301–328.

Ghosh, S., and Lasko, P. (2015). Loss-of-function analysis reveals distinct requirements of the translation initiation factors eIF4E, eIF4E-3, eIF4G and eIF4G2 in *Drosophila* spermatogenesis. PLoS One **10**:e0122519.

Grierson, C., Nielsen, E., Ketelaarc, T., and Schiefelbein, J. (2014). Root hairs. Arabidopsis Book **12**:e0172.

Gutiérrez, R.A., Ewing, R.M., Cherry, J.M., and Green, P.J. (2002). Identification of unstable transcripts in *Arabidopsis* by cDNA microarray analysis: rapid decay is associated with a group of touch and specific clock-controlled genes. Proc. Natl. Acad. Sci. U S A **99**:11513–11518.

Haghighat, A., and Sonenberg, N. (1997). eIF4G dramatically enhances the binding of eIF4E to the mRNA5-cap structure. J. Biol. Chem. **272**:21677–21680.

Haruta, M., Sabat, G., Stecker, K., Minkoff, B.B., and Sussman, M.R. (2014). A peptide hormone and its receptor protein kinase regulate plant cell expansion. Science **343**:408–411.

Haruta, M., Gaddameedi, Vet., Burch, H., Fernandez, D., and Sussman, M.R. (2018). Comparison of the effects of a kinase-dead mutation of FERONIA on ovule fertilization and root growth of *Arabidopsis*. FEBS Lett. **592**:2395–2402.

Henderson, M.A., Cronland, E., Dunkelbarger, S., Contreras, V., Strome, S., and Keiper, B.D. (2009). A germline-specific isoform of eIF4E (IFE-1) is required for efficient translation of stored mRNAs and maturation of both oocytes and sperm. J. Cell Sci. **122**:1529–1539.

Hepler, P.K., Vidali, L., and Cheung, A. (2001). Polarized cell growth in higher plants. Annu. Rev. Cell Dev. Biol. **17**:159–187.

Hernández, G., Han, H., Gandin, V., Fabian, L., Ferreira, T., Zuberek, J., Sonenberg, N., Brill, J.A., and Lasko, P. (2012). Eukaryotic initiation factor 4E-3 is essential for meiotic chromosome segregation, cytokinesis and male fertility in *Drosophila*. Development **139**:3211–3220.

Hwang, Y., Choi, H., Cho, H., and Cho, H. (2017). Tracheophytes contain conserved orthologs of a basic helix-loop-helix transcription factor that modulate ROOT HAIR SPECIFIC genes. Plant Cell. **29**:39–53.

Jones, M.A., Shen, J.J., Fu, Y., Li, H., Yang, Z., and Grierson, C.S. (2002). The *Arabidopsis* Rop2 GTPase is a positive regulator of both root hair initiation and tip growth. Plant Cell **14**:763–776.

Karas, B., Amyot, L., Johansen, C., Sato, S., Tabata, S., Kawaguchi, M., and Szczyglowski, K. (2009). Conservation of lotus and *Arabidopsis* basic helix-loop-helix proteins reveals new players in root hair development. Plant Physiol. **151**:1175–1185.

Kessler, S.A., Shimosato-Asano, H., Keinath, N.F., Wuest, S.E., Ingram, G., Panstruga, R., and Grossniklaus, U. (2010). Conserved molecular components for pollen tube reception and fungal invasion. Science **330**:968–971.

Kim, D.S., Kim, N.H., and Hwang, B.K. (2015). GLYCINE-RICH RNA-BINDING PROTEIN1 interacts with RECEPTOR-LIKE CYTOPLASMIC PROTEIN KINASE1 and suppresses cell death and defense responses in pepper (*Capsicum annuum*). New Phytol. **205**:786–800.

Klumpp, S., Scott, M., Pedersen, S., and Hwa, T. (2013). Molecular crowding limits translation and cell growth. Proc. Natl. Acad. Sci. U S A **110**:16754–16759.

Li, C., Yeh, F., Cheung, A., Duan, Q., Kita, D., Liu, M., Maman, J., Luu, E., Wu, B., Gates, L., et al. (2015). Glycosylphosphatidylinositol-anchored proteins as chaperones and co-receptors for FERONIA receptor kinase signaling in Arabidopsis. Elife **4**:e06587.

Li, C., Cheung, A., and Wu, H. (2016). FERONIA and her pals: functions and mechanisms. Plant Physiol. **171**:2379–2392.

Li, C., Liu, X., Qiang, X., Li, X., Zhu, S., Wang, L., Wang, Y., Liao, H., Luan, S., and Feng, Y. (2018). EBP1 nuclear accumulation negatively feeds back on FERONIA-mediated RALF1 signaling. PLoS Biol. **16**:e2006340.

Liao, H., Tang, R., Zhang, X., Luan, S., and Feng, Y. (2017). FERONIA receptor kinase at the crossroads of hormone signaling and stress responses. Plant Cell Physiol. **58**:1143–1150.

Liu, H., Yu, X., Li, K., Klejnot, J., Yang, H., Lisiero, D., and Lin, C. (2008). Photoexcited CRY2 interacts with CIB1 to regulate transcription and floral initiation in *Arabidopsis*. Science **322**:1535–1539.

Mangano, S., Denita-Juarez, S., Choi, H., Marzol, E., Hwang, Y., Ranocha, P., Velasquez, S., Borassi, C., Barberini, M., Aptekmann, A., et al. (2017). Molecular link between auxin and ROS-mediated polar growth. Proc. Natl. Acad. Sci. U S A **114**:5289–5294.

Mao, D., Yu, F., Li, J., Van de Poel, B., Tan, D., Li, J., Liu, Y., Li, X., Dong, M., Chen, L., et al. (2015). FERONIA receptor kinase interacts with S-adenosylmethionine synthetase and suppresses S-adenosylmethionine production and ethylene biosynthesis in *Arabidopsis*. Plant Cell Environ. **38**:2566–2574.

Marshall, W., Young, K., Swaffer, M., Wood, E., Nurse, P., Kimura, A., Frankel, J., Wallingford, J., Walbot, V., Qu, X., et al. (2012). What determines cell size. BMC Biol. **10**:101.

Menand, B., Yi, K., Jouannic, S., Hoffmann, L., Ryan, E., Linstead, P., Schaefer, D., and Dolan, L. (2007). An ancient mechanism controls the development of cells with a rooting function in land plants. Science **316**:1477–1480.

Miras, M., Truniger, V., Silva, C., Verdaguer, N., Aranda, M., and Querol-Audí, J. (2017). Structure of eIF4E in complex with an eIF4G peptide supports a bipartite binding mode for protein translation. Plant Physiol. **174**:1476–1491.

Missra, A., and von Arnim, A. (2014). Analysis of mRNA translation states in *Arabidopsis* over the diurnal cycle by polysome microarray. Methods Mol. Biol. **1158**:157–174.

Molendijk, A.J., Bischoff, F., Rajendrakumar, C.S., Friml, J., Braun, M., Gilroy, S., and Palme, K. (2001). *Arabidopsis thaliana* RopGTPases are localized to tips of root hairs and control polar growth. EMBO J. **20**:2779–2788.

Nibau, C., Wu, H., and Cheung, A. (2006). RAC/ROP GTPases: 'hubs' for signal integration and diversification in plants. Trends Plant Sci. **11**:309–315.

Nicaise, V., Joe, A., Jeong, B.R., Korneli, C., Boutrot, F., Westedt, I., Staiger, D., Alfano, J.R., and Zipfel, C. (2013). Pseudomonas HopU1 modulates plant immune receptor levels by blocking the interaction of their mRNAs with GRP7. EMBO J. **32**:701–712.

Niedzwiecka, A., Marcotrigiano, J., Stepinski, J., Jankowska-Anyszka, M., Wyslouch-Cieszynska, A., Dadlez, M., Gingras, A., Mak, P., Darzynkiewicz, E., Sonenberg, N., et al. (2002). Biophysical studies of eIF4E cap-binding protein: recognition of mRNA 5′ cap structure and synthetic fragments of eIF4G and 4E-BP1 proteins. J. Mol. Biol. **319**:615–635.

Osborne, M.J., Volpon, L., Kornblatt, J.A., Culjkovic-Kraljacic, B., Baguet, A., and Borden, K.L. (2013). eIF4E3 acts as a tumor suppressor by utilizing an atypical mode of methyl-7-guanosine cap recognition. Proc. Natl. Acad. Sci. U S A **110**:3877–3882.

Patrick, R., and Browning, K. (2012). The eIF4F and eIFiso4F complexes of plants: an evolutionary perspective. Comp. Funct. Genomics **2012**:287814.

Rodriguez, A., Czaplinski, K., Condeelis, J., and Singer, R. (2008). Mechanisms and cellular roles of local protein synthesis in mammalian cells. Curr. Opin. Cell Biol. **20**:144–149.

Roy, A., Kucukural, A., and Zhang, Y. (2010). I-TASSER: a unified platform for automated protein structure and function prediction. Nat. Protoc. **5**:725–738.

Shahbazian, D., Roux, P.P., Mieulet, V., Cohen, M.S., Raught, B., Taunton, J., Hershey, J.W., Blenis, J., Pende, M., and Sonenberg, N. (2006). and Nahum Sonenberg. The mTOR/PI3K and MAPK pathways converge on eIF4B to control its phosphorylation and activity. EMBO J **25**:2781–2791.

Shigeoka, T., Jung, H., Jung, J., Turner-Bridger, B., Ohk, J., Lin, J., Amieux, P., and Holt, C. (2016). Dynamic axonal translation in developing and mature visual circuits. Cell **166**:181–192.

Sonenberg, N., and Hinnebusch, A. (2007). Hinnebusch, New modes of translational control in development, behavior, and disease. Mol. Cell **28**:721–729.

Stegmann, M., Monaghan, J., Smakowska-Luzan, E., Rovenich, H., Lehner, A., Holton, N., Belkhadir, Y., and Zipfel, C. (2017). The receptor kinase FER is a RALF-regulated scaffold controlling plant immune signaling. Science **355**:287–289.

Szostak, E., and Gebauer, F. (2012). Translational control by 3′-UTR-binding proteins. Brief. Funct. Genomics **12**:58–65.

Takeda, S., Gapper, C., Kaya, H., Bell, E., Kuchitsu, K., and Dolan, L. (2008). Local positive feedback regulation determines cell shape in root hair cells. Science **319**:1241–1244.

Timpano, S., and Uniacke, J. (2016). Human cells cultured under physiological oxygen utilize two cap-binding proteins to recruit distinct mRNAs for translation. J. Biol. Chem. **291**:10772–10782.

Tomoo, K., Shen, Xu., Okabe, K., Nozoe, Y., Fukuhara, S., Morino, S., Ishida, T., Taniguchi, T., Hasegawa, H., Terashima, A., et al. (2002). Crystal structures of 7-methylguanosine 5′-triphosphate (m7GTP)- and P1-7-methylguanosine-P3-adenosine-5′,5′-triphosphate (m7GpppA)-bound human full-length eukaryotic initiation factor 4E: biological importance of the C-terminal flexible region. Biochem. J. **362**:539–544.

Uniacke, J., Holterman, C.E., Lachance, G., Franovic, A., Jacob, M.D., Fabian, M.R., Payette, J., Holcik, M., Pause, A., and Lee, S. (2012). An oxygen-regulated switch in the protein synthesis machinery. Nature **486**:126–129.

Véry, A., and Davies, J. (2000). Hyperpolarization-activated calcium channels at the tip of *Arabidopsis* root hairs. Proc. Natl. Acad. Sci. U S A **97**:9801–9806.

Vijayakumar, P., Datta, S., and Dolan, L. (2016). ROOT HAIR DEFECTIVE SIX-LIKE4 (RSL4) promotes root hair elongation by transcriptionally regulating the expression of genes required for cell growth. New Phytol. **212**:944–953.

Waese, J., Fan, J., Pasha, A., Yu, H., Fucile, G., Shi, R., Cumming, M., Kelley, L., Sternberg, M., Krishnakumar, V., et al. (2017). ePlant: visualizing and exploring multiple levels of data for hypothesis generation in plant biology. Plant Cell **8**:1806–1821.

Xiao, Y., Stegmann, M., Han, Z., DeFalco, T., Parys, K., Xu, L., Belkhadir, Y., Zipfel, C., and Chai, J. (2019). Mechanisms of RALF peptide perception by a heterotypic receptor complex. Nature **572**:270–274.

Xu, T., Dai, N., Chen, J., Nagawa, S., Cao, M., Li, H., Zhou, Z., Chen, X., Rycke, R., Rakusová, H., et al. (2014). Cell surface ABP1-TMK auxin-sensing complex activates ROP GTPase signaling. Science **343**:1025–1028.

Yang, J., Roy, A., and Zhang, Y. (2013). Protein-ligand binding site recognition using complementary binding-specific substructure comparison and sequence profile alignment. Bioinformatics **29**:2588–2595.

Yarunin, A., Harris, R.E., Ashe, M.P., and Ashe, H.L. (2011). Patterning of the *Drosophila* oocyte by a sequential translation repression program involving the d4EHP and Belle translational repressors. RNA Biol. **8**:904–912.

Yi, K., Menand, B., Bell, E., and Dolan, L. (2010). A basic helix-loop-helix transcription factor controls cell growth and size in root hairs. Nat. Genet. **42**:264–267.

Yu, F., Qian, L., Nibau, C., Duan, Q., Kita, D., Levasseur, K., Li, X., Lu, C., Li, H., Hou, C., et al. (2012). FERONIA receptor kinase pathway suppresses abscisic acid signaling in *Arabidopsis* by activating ABI2 phosphatase. Proc. Natl. Acad. Sci. U S A **109**:14693–14698.

Yu, F., Li, J., Huang, Y., Liu, L., Li, D., Chen, L., and Luan, S. (2014). FERONIA receptor kinase controls seed size in *Arabidopsis thaliana*. Mol. Plant **7**:920–922.

Zhang, C., Freddolino, P.L., and Zhang, Y. (2017). COFACTOR: improved protein function prediction by combining structure, sequence and protein-protein interaction information. Nucleic Acids Res. **45**:W291–W299.

Zheng, Z., and Yang, Z. (2000). The RopGTPase: an emerging signaling switch in plants. Plant Mol. Biol. **44**:1–9.